ELSEVIER

Neuroscience Letters 356 (2004) 25–28

Neuroscience Letters

www.elsevier.com/locate/neulet

Hydrogen peroxide modulates whole cell Ca^{2+} currents through L-type channels in cultured rat dentate granule cells

Tatsuhiro Akaishi[a,b], Ken Nakazawa[b], Kaoru Sato[b], Hiroshi Saito[a], Yasuo Ohno[b], Yoshihisa Ito[a,*]

[a] *Department of Pharmacology, College of Pharmacy, Nihon University, 7-7-1 Narashinodai, Funabashi-shi, Chiba 274-8555, Japan*
[b] *Division of Pharmacology, National Institute of Health Sciences, Setagaya, Tokyo 158-8501, Japan*

Received 23 October 2003; received in revised form 12 November 2003; accepted 13 November 2003

Abstract

Modification of voltage-gated Ca^{2+} channels by hydrogen peroxide, a membrane-permeable form of reactive oxygen species, in cultured dentate granule cells was examined using the whole cell patch clamp technique. Pretreatment with hydrogen peroxide (1 and 10 μM) for 2 h enhanced the Ca^{2+} current without affecting its voltage dependence. The enhancement was completely cancelled by 1 mM glutathione, an antioxidant, and 2 μM nifedipine, an L-type Ca^{2+} channel blocker. In contrast, the enhancement of the Ca^{2+} current was not mimicked by pretreatment with 10 μg/ml tunicamycin, an endoplasmic reticulum stressor. These results suggest that oxidative stress induced by hydrogen peroxide selectively regulates the activity of L-type Ca^{2+} channels.

Keywords: Hydrogen peroxide; Oxidative stress; Patch clamp; Ca^{2+} channel; Hippocampus; Dentate granule cell

Oxidative stress is implicated in many different neurodegenerative diseases, such as Alzheimer's disease (AD) [16], Parkinson's disease [17], and sporadic amyotrophic lateral sclerosis [13]. Oxidative stress arising from excessive production or decreased clearance of reactive oxygen species (ROS) can result in accumulation of ROS, cellular damage, and eventual cell death. Indeed, molecular and cellular events underlying neuronal death induced by oxidative stress have been demonstrated in the hippocampal cell line HT-22 and in cortical neurons [3,4,14]. Endogenous glutamate depletes intracellular glutathione (GSH), leading to the accumulation of ROS and an increase in Ca^{2+} influx, which finally causes neuronal death. It has been reported that apomorphine, a dopamine D_4 agonist, inhibits oxidative stress-induced neuronal cell death in HT-22 cells and primary rat cortical neurons [3], and the protective effects of apomorphine on cell death are mediated, at least in part, by regulation of the cGMP-operated Ca^{2+} channel. This report also suggests that ROS-induced Ca^{2+} influx plays important roles in oxidative stress-mediated neuronal damage. Several pathways can lead to such Ca^{2+} elevation in neurons, and a major pathway for Ca^{2+} influx across the plasma membrane is voltage-gated Ca^{2+} channels (VGCCs). VGCCs are involved in various neuronal functions, including neurotransmitter release, synaptic plasticity, and gene expression [11]. Excessive Ca^{2+} influx through these channels contributes to neuronal death in pathological settings such as AD [5,11]. Recent studies have demonstrated that hydrogen peroxide (H_2O_2), a membrane-permeable form of ROS, modulates the activities of several types of ion channels [12,15] and these changes in channel activities may also be related to pathological events. Despite the importance of VGCCs, modulation of Ca^{2+} channel activity by oxidative stress has not been adequately studied. To clarify whether ROS alter Ca^{2+} channel activity, we used the whole cell patch clamp technique to examine the effects of H_2O_2 on VGCCs in cultured dentate granule cells from postnatal rats.

All experiments in this study were performed in accordance with the guidelines of the National Institute of Health Sciences. For the preparation of cultured dentate granule cells, we employed with modification a cell culture system described by Ikegaya et al. [2]. Briefly, 3- to 4-day-old Wistar rat pups (Nihon SLC, Shizuoka, Japan) were deeply anesthetized with ether, and the hippocampi were removed. The dentate gyrus was dissected out and incubated with 0.25% trypsin (Difco, Detroit, MI) and 0.01%

* Corresponding author. Tel./fax: +81-474-65-5832.
E-mail address: yoshiito@pha.nihon-u.ac.jp (Y. Ito).

0304-3940/03/$ - see front matter © 2003 Elsevier Ireland Ltd. All rights reserved.
doi:10.1016/j.neulet.2003.11.012

deoxyribonuclease I (Sigma, St Louis, MO) at 37 °C for 30 min. The pellet was suspended in a mixture of 50% Neurobasal medium (Life Technologies, Gaithersburg, MD) containing 2% B-27 supplement (Life Technologies) and 73 μg/ml L-glutamine (Wako, Osaka, Japan), and 50% astrocyte-conditioned medium. The suspension was gently triturated, and passed through two sheets of nylon net. The cells were plated at a density of 2.0×10^4 cells/cm^2 onto 13 mm round glass coverslips (Matsunami, Osaka, Japan) coated with polyethyleneimine. One day after the plating, the ACM-containing medium was changed to ACM-free Neurobasal medium containing 2% B-27 supplement and 73 μg/ml L-glutamine. The medium was changed twice a week thereafter. The cells were cultured at 37 °C in a humidified 5% CO_2/95% air atmosphere.

Electrophysiological experiments were performed with cells that had been cultured for 7–9 days. Immediately before experimental treatment, the culture medium was replaced with Locke's solution (154 mM NaCl, 5.6 mM KCl, 2.3 mM $CaCl_2$, 1.0 mM $MgCl_2$, 3.6 mM $NaHCO_3$, 10 mM glucose, and 5.0 mM HEPES, pH 7.2) according to Mark et al. [10]. H_2O_2 (Sigma) was freshly prepared daily. GSH-ethyl ester (Sigma) and tunicamycin (Sigma) were prepared as 100 × stock solutions in saline. Responses were recorded at room temperature using the whole cell recording configuration of the patch clamp technique with an amplifier (Nihon Kohden, Tokyo, Japan) and data acquisition software (pCLAMP; Axon Instruments, CA, USA). Electrical signals were filtered at 1 kHz. Glass pipettes (2–5 MΩ) were filled with 100 mM CsCl, 2.0 mM $MgCl_2$, 10 mM EGTA, 10 mM HEPES, 15 mM tetraethylammonium chloride, 5 mM Mg-ATP, 20 mM creatine phosphate and 50 units/ml creatine kinase (pH 7.3). Unless otherwise indicated, the recording medium contained the following: 130 mM NaCl, 5.0 mM $CaCl_2$, 2.0 mM $MgCl_2$, 10 mM HEPES, 10 mM glucose, 5.0 mM 4-aminopyridine and 500 nM tetrodotoxin (pH 7.4). Drugs used for the isolation of different Ca^{2+} currents were added to the external solution.

For electrophysiological experiments, cells were carefully selected from cultures according to their morphological characteristics (Fig. 1A, left). The cells were small in size (the average diameter was about 9 μm) and round or oval in shape, consistent with the morphological characteristics of dentate granule cells reported in a previous study [1]. Ca^{2+} currents in the cells were recorded with Cs^+-based pipette solution (Fig. 1A, right). Ca^{2+} currents elicited by depolarizing voltage steps between −50 and +80 mV are shown in Fig. 1B (open circles). Voltage steps were applied for 100 ms from a holding potential of −50 mV. The currents activated around −30 mV, peaked at 0 mV, and reversed around +50 mV. Their kinetics compare well with those of the high voltage-activated (HVA) Ca^{2+} currents reported by Eliot and Johnston [1]. We examined the effects of H_2O_2 on VGCCs in these cells. Pretreatment of the cells with H_2O_2 (1 and 10 μM) for 2 h resulted in a significant increase in the amplitude of the Ca^{2+} current (Fig. 1B,C).

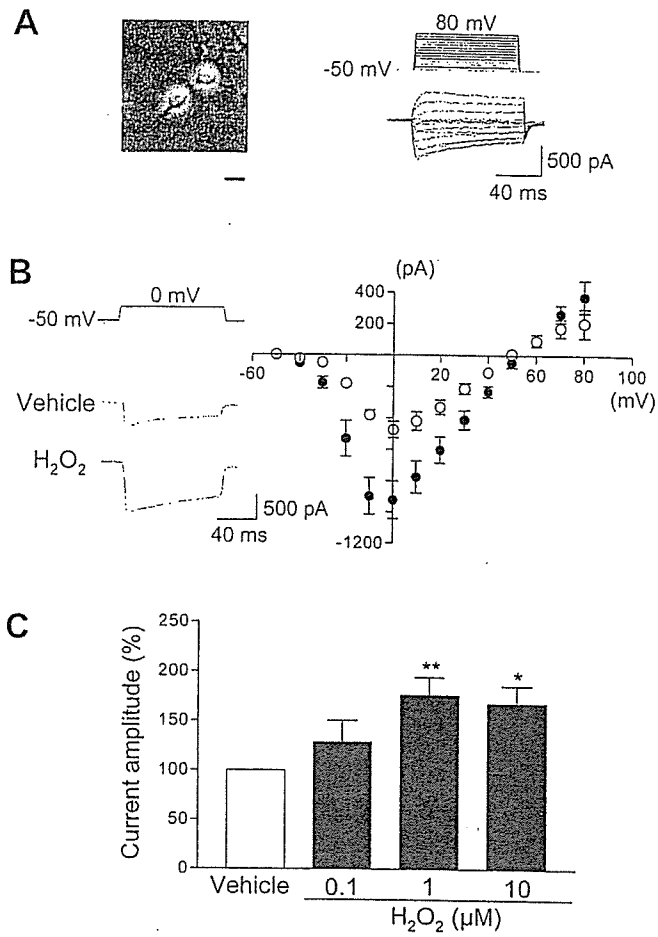

Fig. 1. H_2O_2 enhances whole cell Ca^{2+} current in cultured rat dentate granule cells. (A) Representative photomicrographs of cultured dentate granule cells 7 days after culture (left). Scale bar, 10 μm. Leak-subtracted Ca^{2+} current in a cell elicited by 100 ms step commands from −50 mV (right). (B) Effects of H_2O_2 on the Ca^{2+} current. Representative recordings of the Ca^{2+} current in cells that had been treated for 2 h with either vehicle or 1 μM H_2O_2 (left). Current–voltage relationship of the Ca^{2+} current in vehicle-treated (○, $n = 9$) and H_2O_2-treated (●, $n = 11$) cells (right). (C) Concentration dependency of the effects of H_2O_2 on Ca^{2+} currents. Values are the mean ± SEM of measurements made in four to 21 neurons in at least three separate cultures (**$P < 0.01$, *$P < 0.05$ vs. the vehicle; ANOVA followed by Dunnett's multiple range test).

For higher concentrations of H_2O_2, it was very difficult to record currents after treatment with 20–200 μM H_2O_2 for 2 h, and no living cells were observed at concentrations higher than 200 μM. We used a concentration of 1 μM to analyze the phenomenon in the following experiments because 1 μM H_2O_2 showed a robust and significant effect. The current–voltage relationships in the absence or presence of H_2O_2 showed that the voltage dependence remained unchanged in cells exposed to H_2O_2 (Fig. 1B).

Five types of HVA Ca^{2+} channels (L-, N-, P-, Q- and R-types) have been identified on the basis of their pharmacological and biophysical properties, and selective blockers are available for L-, N-, and P/Q-type Ca^{2+} channels. To determine which types of VGCCs were affected by H_2O_2, we employed blockers of specific channel types. In vehicle-

treated cultures, addition of 2 μM nifedipine (a blocker of L-type Ca^{2+} channels; Sigma), 3 μM ω-conotoxin-GVIA (a blocker of N-type Ca^{2+} channels; Peptides Institute, Osaka, Japan) and 0.3 μM ω-agatoxin-IVA (a blocker of P/Q-type Ca^{2+} channels; Peptides Institute) resulted in a 29.5%, 19.4% and 22.9% decrease in the amplitude of the Ca^{2+} current, respectively (Fig. 2). In H_2O_2-treated neurons, nifedipine caused a 92.8% decrease, ω-conotoxin-GVIA caused a 18.9% decrease, and ω-agatoxin-IVA caused a 22.9% decrease in the Ca^{2+} current amplitude (Fig. 2B), indicating that the H_2O_2-induced enhancement of the Ca^{2+} current was selectively blocked by nifedipine.

Oxidative stress-induced neuronal damage is associated with a decrease of intracellular GSH. It has been shown that a decrease in the GSH level causes the accumulation of intracellular ROS, resulting in Ca^{2+} influx from the extracellular medium [3,4,14]. To investigate whether intracellular GSH prevents H_2O_2-induced enhancement of the Ca^{2+} current, we examined the effects of GSH-ethyl ester, a membrane-permeable form of GSH, on the current. As shown in Fig. 3A, there was no increase in the Ca^{2+} current amplitude when cells were treated with 1 mM GSH-ethyl ester and 1 μM H_2O_2 simultaneously. It has been shown that not only oxidative stress but also endoplasmic reticulum (ER) stress plays a role in neuronal cell death [6–8]. In these

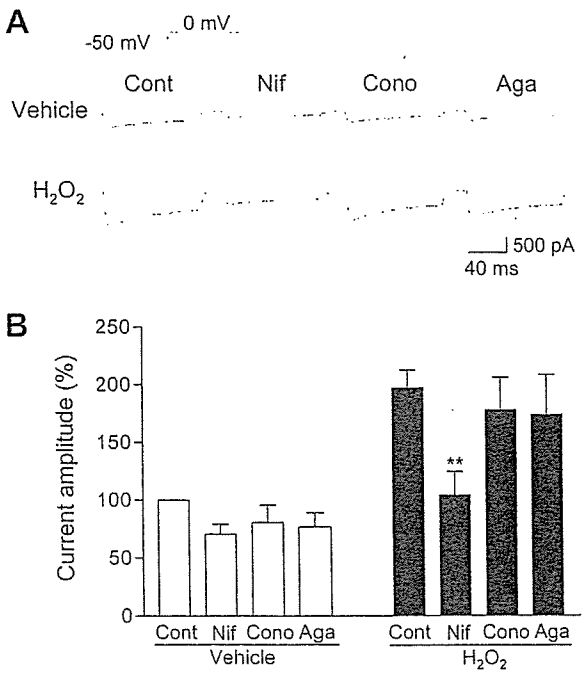

Fig. 2. Effects of Ca^{2+} channel blockers on the amplitude of the Ca^{2+} current in cultured dentate granule cells. (A) Representative recordings of the Ca^{2+} current in the cells. (B) Summarized data of current amplitudes obtained in the absence (Cont) or presence of blockers of specific subtypes of VGCCs (nifedipine, Nif; ω-conotoxin-GVIA, Cono; ω-agatoxin-IVA, Aga) from vehicle-treated (vehicle) and 1 μM H_2O_2-treated (H_2O_2) cells. Values are the mean ± SEM of measurements made in five to 19 neurons in at least three separate cultures (**$P < 0.01$ vs. Cont; ANOVA followed by Dunnett's multiple range test).

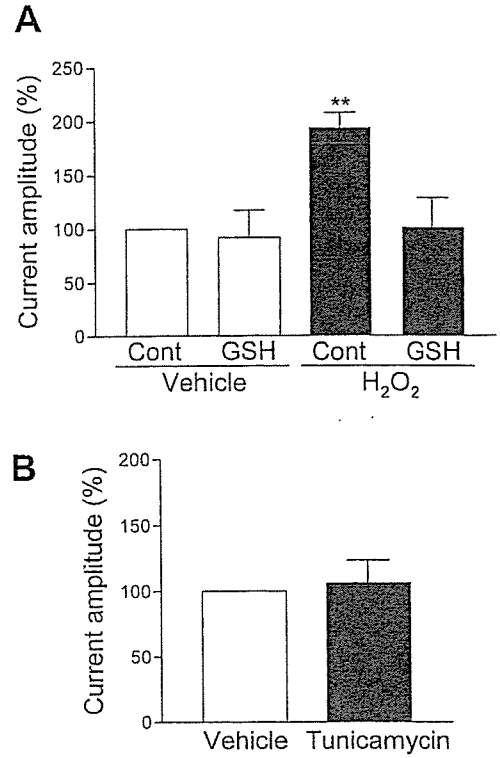

Fig. 3. Effects of simultaneous treatment with GSH and H_2O_2 (A) and tunicamycin (B) on the Ca^{2+} current. Cells were exposed for 2 h to the indicated agents, and whole cell Ca^{2+} current was recorded. (A) GSH-ethyl ester (1 mM) attenuated the H_2O_2 (1 μM)-induced enhancement of the Ca^{2+} current. The values are the means ± SEM of measurements made in five to ten neurons in at least three separate cultures (**$P < 0.01$ vs. the vehicle (Cont); ANOVA followed by Dunnett's multiple range test). (B) Tunicamycin (10 μg/ml) does not affect the Ca^{2+} current. The values are the means ± SEM of measurements made in four neurons in at least three separate cultures.

studies, amyloid β-protein- and tunicamycin (an inhibitor of *N*-glycosylation in the ER)-induced cell death was triggered by ER dysfunction in cultured hippocampal neurons and PC12 cells. We examined the effects of tunicamycin on Ca^{2+} currents in the dentate granule cells. Unlike H_2O_2, tunicamycin (10 μg/ml) induced no current enhancement (Fig. 3B). This result suggests that oxidative stress, but not ER stress, modulates the Ca^{2+} channel activities in these cells.

In the present study, we have demonstrated that pretreatment with H_2O_2 enhances the Ca^{2+} current through L-type Ca^{2+} channels in dentate granule cells. This is the first report to provide direct evidence that H_2O_2 modifies L-type Ca^{2+} channel activity in these cells. The enhancement of the Ca^{2+} current was completely prevented by cotreatment with GSH-ethyl ester. The results are suggestive of involvement of H_2O_2 in modulation of Ca^{2+} channel activities. It has already been reported that H_2O_2 inhibits voltage-gated K^+ channels [12] and $GABA_A$-gated Cl^- channels in rat hippocampal neurons [15]. Our data showing that H_2O_2 did not affect the activity of P/Q-type Ca^{2+} channels are in contrast to a previous report showing that

H_2O_2 enhanced Ca^{2+} currents through P/Q-type Ca^{2+} channels composed of α1A, α2/δ, and β3 subunits at potentials more negative than 0 mV [9]. The discrepancy may be due to differences in experimental conditions. For example, we examined the Ca^{2+} current of cultured dentate granule cells, whereas the previous study measured the current permeating through cloned neuronal Ca^{2+} channels expressed in *Xenopus* oocytes.

The exact mechanisms whereby H_2O_2 selectively enhances the nifedipine-sensitive Ca^{2+} current still remain to be elucidated. Pretreatment with the ER stressor tunicamycin did not affect the Ca^{2+} current. Taken together, these results suggest that oxidative stress may selectively regulate the activity of L-type Ca^{2+} channels in dentate granule cells. Currents through VGCCs are known to be increased by phosphorylation of channel α subunit proteins [18]. H_2O_2 may directly or indirectly increase phosphorylation of the α subunit of L-type Ca^{2+} channels.

Acknowledgements

This work was partly supported by Health and Labour Science Research Grants for Research on Advanced Medical Technology from the Ministry of Health, Labour and Welfare, Japan and a grant-in-aid for scientific research from the Ministry of Education, Culture, Sports, Science, and Technology, Japan (KAKENHI13672319) awarded to K.K.

References

[1] L.S. Eliot, D. Johnston, Multiple components of calcium current in acutely dissociated dentate gyrus granule neurons, J. Neurophysiol. 72 (1994) 762–777.
[2] Y. Ikegaya, N. Nishiyama, N. Matsuki, L-Type Ca^{2+} channel blocker inhibits mossy fiber sprouting and cognitive deficits following pilocarpine seizures in immature mice, Neuroscience 98 (2000) 647–659.
[3] K. Ishige, Q. Chen, Y. Sagara, D. Schubert, The activation of dopamine D4 receptors inhibits oxidative stress-induced nerve cell death, J. Neurosci. 21 (2001) 6069–6076.
[4] K. Ishige, D. Schubert, Y. Sagara, Flavonoids protect neuronal cells from oxidative stress by three distinct mechanisms, Free Radic. Biol. Med. 30 (2001) 433–446.
[5] K. Ito, K. Nakazawa, S. Koizumi, M. Liu, K. Takeuchi, T. Hashimoto, Y. Ohno, K. Inoue, Inhibition by antipsychotic drugs of L-type Ca^{2+} channel current in PC12 cells, Eur. J. Pharmacol. 314 (1996) 143–150.
[6] Y. Ito, M. Arakawa, K. Ishige, H. Fukuda, Comparative study of survival signal withdrawal and hydroxymonenal-induced cell death in cerebellar granule cells, Neurosci. Res. 35 (1999) 321–327.
[7] Y. Ito, Y. Kosuge, T. Sakikubo, K. Horie, N. Ishikawa, N. Obokata, E. Yokoyama, K. Yamashina, M. Yamamoto, H. Saito, M. Arakawa, K. Ishige, Protective effect of S-allyl-L-cysteine, a garlic compound, on amyloid β-protein-induced cell death in nerve growth factor-differentiated PC12 cells, Neurosci. Res. 46 (2003) 119–125.
[8] Y. Kosuge, Y. Koen, K. Ishige, K. Minami, H. Urasawa, H. Saito, Y. Ito, S-Allyl-L-cysteine selectively protects cultured rat hippocampal neurons from amyloid β-protein- and tunicamycin-induced neuronal death, Neuroscience (2004) in press.
[9] A. Li, J. Segui, S.H. Heinemann, T. Hoshi, Oxidation regulates cloned neuronal voltage-dependent Ca^{2+} channels expressed in *Xenopus* oocytes, J. Neurosci. 18 (1998) 6740–6747.
[10] R.J. Mark, M.A. Lovell, W.R. Markesbery, K. Uchida, M.P. Mattson, A role for 4-hydroxynonenal, an aldehydic product of lipid peroxidation, in disruption of ion homeostasis and neuronal death induced by amyloid β-peptide, J. Neurochem. 68 (1997) 255–264.
[11] G.P. Miljanich, J. Ramachandran, Antagonists of neuronal calcium channels: structure, function, and therapeutic implications, Annu. Rev. Pharmacol. Toxicol. 35 (1995) 707–734.
[12] W. Müller, K. Bittner, Differential oxidative modulation of voltage-dependent K^+ currents in rat hippocampal neurons, J. Neurophysiol. 87 (2002) 2990–2995.
[13] W.A. Pedersen, W. Fu, J.N. Keller, W.R. Markesbery, S. Appel, R.G. Smith, E. Kasarskis, M.P. Mattson, Protein modification by the lipid peroxidation product 4-hydroxynonenal in the spinal cords of amyotrophic lateral sclerosis patients, Ann. Neurol. 44 (1998) 819–824.
[14] Y. Sagara, K. Ishige, C. Tsai, P. Maher, Tyrphostins protect neuronal cells from oxidative stress, J. Biol. Chem. 277 (2002) 36204–36215.
[15] R. Sah, F. Galeffi, R. Ahrens, G. Jordan, R.D. Schwartz-Bloom, Modulation of the $GABA_A$-gated chloride channel by reactive oxygen species, J. Neurochem. 80 (2002) 383–391.
[16] B.A. Yankner, Mechanisms of neuronal degeneration in Alzheimer's disease, Neuron 16 (1996) 921–932.
[17] A. Yoritaka, N. Hattori, K. Uchida, M. Tanaka, E.R. Stadtman, Y. Mizuno, Immunohistochemical detection of 4-hydroxynonenal protein adducts in Parkinson disease, Proc. Natl. Acad. Sci. USA 93 (1996) 2696–2701.
[18] G.W. Zamponi, E. Bourinet, D. Nelson, J. Nargeot, T.P. Snutch, Crosstalk between G proteins and protein kinase C mediated by the calcium channel α1 subunit, Nature 385 (1997) 442–446.

Available online at www.sciencedirect.com
SCIENCE DIRECT®
Biochemical and Biophysical Research Communications 315 (2004) 603–611
BBRC
www.elsevier.com/locate/ybbrc

A novel function of N-cadherin and Connexin43: marked enhancement of alkaline phosphatase activity in rat calvarial osteoblast exposed to sulfated hyaluronan

Misao Nagahata,[a,b,*] Toshie Tsuchiya,[b] Tatsuya Ishiguro,[a] Naoki Matsuda,[c] Yukio Nakatsuchi,[d] Akira Teramoto,[a] Akira Hachimori,[e] and Koji Abe[a]

[a] *Department of Functional Polymer Science, Faculty of Textile Science and Technology, Shinshu University, Ueda 386-8567, Japan*
[b] *Division of Medical Devices, National Institute of Health Sciences, Kamiyoga 158-8501, Japan*
[c] *Radioisotope Center, Nagasaki University, Nagasaki 852-8526, Japan*
[d] *Department of Orthopaedic Surgery, National Nagano Hospital, Ueda 386-8610, Japan*
[e] *Institute of High Polymer Research, Faculty of Textile Science and Technology, Shinshu University, Ueda 386-8567, Japan*

Received 6 January 2004

Abstract

In this study, we examined the interaction of the osteoblast which forms bone and sulfated hyaluronan (SHya). For the purpose of the creation of a new functional polysaccharide, we introduced a sulfate group in hyaluronan (Hya) of high molecular weight, and SHya of high molecular weight could be obtained for the first time. When rat calvarial osteoblast (rOB) cells were cultured with a high concentration of SHya, they formed aggregated spheroids after 4 h and the spheroids grew to about 200 μm after 24 h. We examined the expression of cell adhesion molecules in order to clarify the mechanism of aggregate formation. The N-cadherin (N-cad) and Connexin43 (Cx43) expression level of rOB cells cultured with SHya remarkably increased after 2 h. A difference in the expression of Integrin β1 (Intβ1) could not be observed between the SHya addition and control group. The alkaline phosphatase (ALPase) activity of rOB cells cultured with SHya after 8 h was significantly enhanced in comparison with control. Therefore, the sulfate group of SHya seems to enhance expression of cell adhesion protein such as N-cad and Cx43, resulting in aggregate formation and further remarkable induction of the ALPase activity of rOB cells.

Keywords: Sulfated hyaluronan; Osteoblast; Aggregation; N-cadherin; Connexin; ALPase activity

It is reported that the extracellular matrix (ECM) provides positional and environmental information essential for tissue function [1]. ECMs are complex, consisting of several different classes of molecules that may regulate modeling and remodeling [2]. Sulfated polysaccharides, such as heparan sulfate (HS) or heparin (Hep), stabilize fibroblast growth factor (FGF) and transforming growth factor β (TGF-β) in an active conformation, protect them against pH, thermal, and proteolytic degradations, and strongly potentiate their mitogenic activity in many cell types. Growth factors play a key role in the process of bone repair [3,4]. However, when the size of the defect is large, growth factor alone is not enough for bone repair. One promising way of promoting bone repair is to use cell scaffold, such as collagen [5]. However, there are problems, such as the antigenicity on the proteins. Therefore, we tried the regeneration of the bone using biocompatibility polysaccharides. Hyaluronan (Hya) has by far the highest molecular weight of the glycosaminoglycans (GAGs) and is thought to facilitate cell migration, adhesion, proliferation, and tissue repair [6].

Then, we synthesized sulfated hyaluronan (SHya) with different degrees of sulfation. We examined the effect of SHya on the cell function of rOB cells.

* Corresponding author. Fax: +81-3-3700-9196.
E-mail address: nagahata@nihs.go.jp (M. Nagahata).

0006-291X/$ - see front matter © 2004 Elsevier Inc. All rights reserved.
doi:10.1016/j.bbrc.2004.01.098

Materials and methods

Sulfated hyaluronan. On the sulfation of the polysaccharide, various methods are reported [7–10]. However, the sugar chain is easily cut off under reaction and the molecular weight lowers. Therefore, a method using sulfur trioxide (SO_3) complex was developed to prevent the lowering of the molecular weight [11–13]. The molecular weight simply lowers on Hya by acid and heating. Then, the synthesis was carried out using dimethylformamide (DMF)–SO_3 complex and trimethylamine (TMA)–SO_3 complex. Hya derivatives with different sulfation degrees can be obtained by changing the amount of DMF–SO_3 complex and TMA–SO_3 complex.

Dimethylformamide–SO_3 complex. Ten percent Hya150 (molecular weight, 1.5×10^6) solution in *N,N*-dimethylformamide (DMF) (WAKO Pure Chemical Industries) was mixed with DMF–SO_3 complex [14] and stirred for 14 h at 0 °C. The reaction mixture was then diluted, neutralized, and precipitated by adding to a large quantity of acetone. The precipitate was dissolved in distilled water again and dialyzed against distilled water.

Trimethylamine–SO_3 complex. Ten percent Hya150 solution in DMF was mixed with TMA–SO_3 complex (Aldrich Chemical) and stirred for 48 h at 60 °C. SHya was obtained after the reaction by the method equal to the above-mentioned DMF–SO_3 complex method.

The degree of substitution (DS) of SHya was 1.2, 2.1, and 3.4 as determined by the chelate titration method [15]. Moreover, the effectiveness of sulfation was also demonstrated by FT-IR analysis. The IR spectrum of SHya exhibited two absorption bands at 1240 and 820 cm^{-1} due to the S=O and SO_3^- stretching, respectively. Characteristics of SHya are summarized in Table 1 and chemical structures are illustrated in Fig. 1. The number, which is at the end of the compound's name, indicates MW [$\times 10^4$] and the subscript shows the DS.

Cell culture. The rOB cells were isolated and cultured using the method described by Hamano et al [16]. rOB cells were cultured in a sterile tissue culture dish (NUNCLON) with the use of Dulbecco's modified Eagle's medium (DMEM, Nissui-seiyaku) supplemented with 10% fetal bovin serum (FBS, Gibco). Cultures were maintained in a 5% CO_2 humidified atmosphere at 37 °C. The cells were plated in 24-well tissue culture plates (NUNCLON) or 100 mm ϕ tissue culture dish (NUNCLON) at an initial density of 5×10^4 cells/cm^2 for study of the effects of Hya and SHya on cell function. The cells were subconfluent after 2–3 days of culture and confluent after 3–4 days.

Table 1
Characteristics of polysaccharides

Polysaccharides	Number of sulfate groups per two saccharide rings	MW ($\times 10^4$)
Hya	0	30
1.2 SHya	1.2	55
2.1 SHya	2.1	20
3.4 SHya	3.4	5

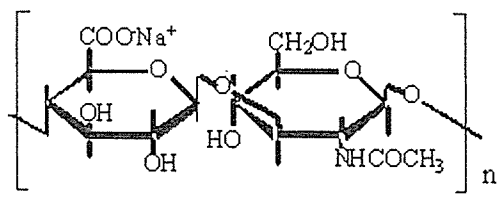

Hyaluronan (Hya)

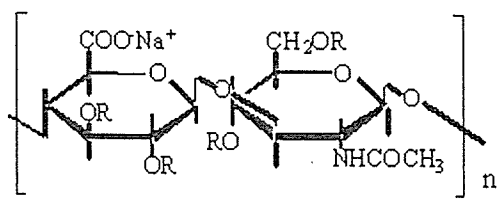

Sulfated hyaluronan (SHya)

R= SO_3Na or H

Fig. 1. Structure of hyaluronan and sulfated hyaluronan.

Western blotting analysis. Immunoblots of N-cadherin (N-cad), Integrin β1 (Intβ1), and Connexin43 (Cx43) were performed according to the method of Matsuda et al. [17]. rOB cells were plated in 100 mm ϕ dishes. The cells were incubated with SHya for different time intervals as indicated in the results, washed with phosphate-buffered saline (PBS (−)), and lysed for 30 min at 4 °C with RIPA buffer. After sonicating the lysates for 30 s using a sonicator, their protein concentrations were determined using DC protein assay (Bio-Rad Laboratories). The lysate was mixed with equal volumes of Laemmli sample buffer, and proteins were separated on 7.5% polyacrylamide gels and transferred to nitrocellulose membranes (OSMONICS). After blocking with 3% nonfat dried milk in Tris-buffered saline with Tween 20 buffer, the membranes were incubated successively with a primary antibody, followed by incubation with antimouse antibodies conjugated with ALP, and detection with ALP detection reagent (Gibco). Primary antibodies used include those recognizing N-cad, Intβ1, and Cx43. All antibodies were monoclonal mouse antibodies and were obtained from BD Transduction Laboratories.

Preparation of cell lysate for assay. Cell lysates were prepared according to the method of Hamano et al. [16]. After removal of the culture medium from the dishes, cells were washed three times with PBS (−). One milliliter of PBS (−) containing 0.04% Nonidet P-40 (Nacalai tesque) was poured into the dishes and incubated at 37 °C for 10 min. The suspension was homogenated with an ultrasonic disrupter (BH-200P, TOMY SEIKO) and centrifuged at 1000 rpm for 10 min at 4 °C. These cell lysates were used as sample solutions for the measurements of protein content and ALPase activity.

Protein content. Total protein content of cell lysate was measured by the BIO-RAD protein assay method (Protein assay, Bio-Rad Laboratories) and absorbance at 595 nm was measured using an ELISA reader (Bio-Rad Laboratories), using bovine serum albumin (WAKO Pure Chemical Industries) as reference standard.

Alkaline phosphatase activity. Alkaline phosphatase (ALPase) activity was determined by the modification of the methods of Hamano et al. [16] and Lowry et al. [18]. The reaction mixture consisted of 0.1 ml cell lysate and 0.4 ml of 16 mM *p*-nitrophenylphosphate disodium salt hexahydrate (WAKO Pure Chemical Industries). The solution was incubated at 37 °C for 30 min. The enzymatic reaction was stopped by adding 0.5 ml of 0.5 N NaOH and absorbance at 410 nm of *p*-nitrophenol liberate was measured. The enzyme activity was expressed in units/mg of protein, where 1 U corresponded to 1 nmol of *p*-nitrophenol liberate per 30 min at 37 °C. For determination of the localization of the ALPase activity, cells were rinsed with PBS (−) and fixed with 10% formalin (pH 7.4) overnight at 4 °C. These fixed dishes were rinsed three times with distilled water and Azo staining solution (5 mg naphthol AS-BI phosphoric acid sodium salt (FLUKA) in 10 ml of 0.05 M 2-amino-2-methyl-1,3-propandiol (WAKO Pure Chemical Industries) buffer (pH 9.8)) for 5 min at room temperature. Finally, they were washed three times with distilled water.

Culture conditions for estimating the interaction of serum and SHya. Four kinds of dishes were prepared as follows: (A) DMEM only, (B) DMEM with 10% FBS, (C) 2.1SHya in DMEM with 10% FBS, and (D) 2.1SHya only in DMEM into 35-mm tissue culture dish (NUNCLON), and incubated for 2 h at 37 °C, respectively. After the incubation, these dishes were washed up with PBS (−) three times. rOB cells were suspended in DMEM without serum, the cell suspensions were added into these dishes, and cell adhesion and morphological change were examined after 24 h-incubation.

Interaction of serum components and SHya. The cells were plated in serum free DMEM supplemented with fibronectin (FN), basic FGF

(bFGF), and SHya. Cells in culture were incubated at 37 °C for 24 h with 5% CO_2.

Results

Fig. 2 shows the morphologies of the attachment of rOB cells cultured with four different concentrations of 2.1SHya after 24 h. rOB cells treated with high concentrations (0.25 and 0.5 mg/ml) of 2.1SHya formed large aggregations. Western blotting was used to examine the effect of 2.1SHya on adhesion protein expression in rOB cells. The cultures were washed with cold PBS (−) and protein samples were collected by the addition of a lysis buffer. As shown in Fig. 3A, the control time-dependently increased protein levels of N-cad, Intβ1 after incubation with rOB cells for 24 h. The time-dependence of 2.1SHya stimulation of N-cad is shown in Fig. 3B. This response was considerably earlier than that observed for the control, peaking 2–6 h after 2.1SHya addition (Fig. 3C). Expression of Intβ1 was not observed in great difference for the 2.1SHya addition and control. Cx43 expression level in the 2.1SHya addition reached a peak at 2–4 h, and increase in some expression levels of protein was observed in comparison with the control (Fig. 3C). N-cadherin in Fig. 4 shows the morphologies of the attachment of rOB cells treated with different DS SHya and Hya after 24 h. Cell aggregations were formed in the case of high DS SHya (2.1SHya, 3.4SHya). In the meantime, with low DS 1.2SHya or nonsulfated Hya, aggregations were not formed. However, when 1.2SHya was added in high density, rOB formed aggregations. Fig. 5 shows rOB cell proliferation in the presence of SHya and Hya. In the presence of 2.1SHya, cell proliferation was suppressed after seeding 48 h. However, rOB cells treated with 2.1SHya gradually proliferated afterwards and it reached confluence after 120 h. Hya showed similar trends in the control (TCD). Fig. 6 shows photographs of the Azo staining used for the determination of ALPase activity localization on rOB cell monolayers and aggregates cultured for 24 h. The staining also immaturely dyed the central part of the aggregation observed in the 2.1SHya. The rOB cells in TCD and Hya did not stain with Azo staining. The ALPase activity was only expressed in the aggregates. Compared with the control and Hya, 2.1SHya also time-dependently enhanced the ALPase activity of rOB cells when examined at a concentration of 0.5 mg/ml (Fig. 7). The effect of the existence of serum component and 2.1SHya on the formation of aggregation of rOB cells was examined (Fig. 8). rOB cells did not form aggregations without 2.1SHya in the case of the serum-free medium (Fig. 8D). The adherent cell number increased when it

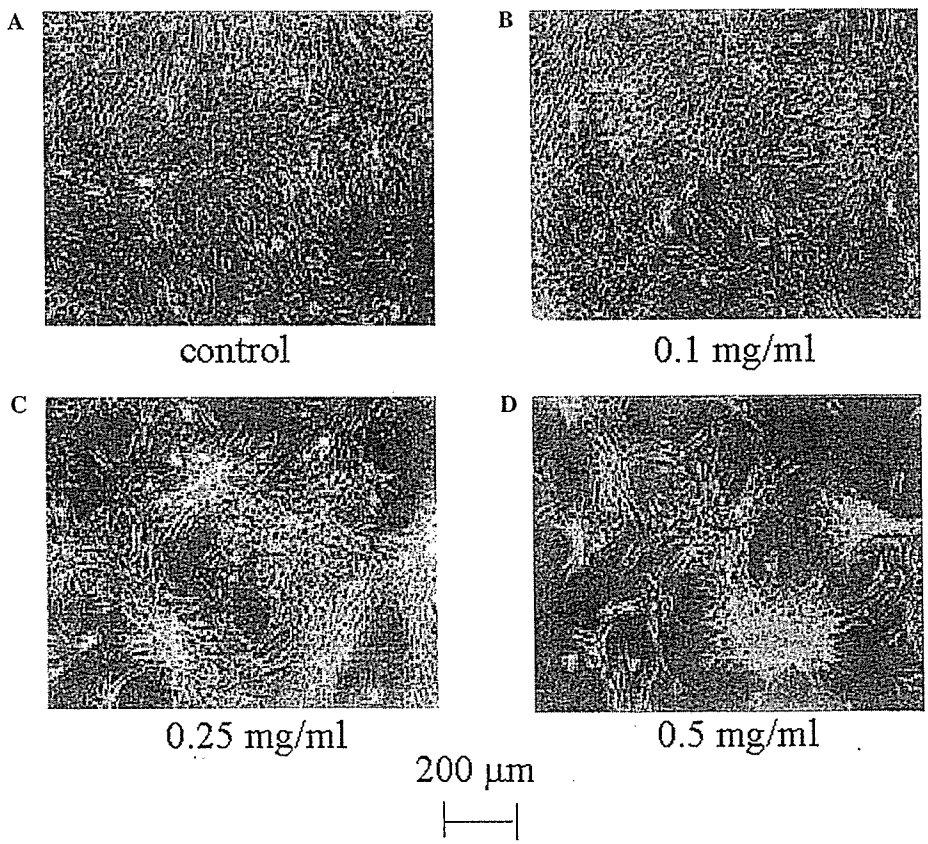

Fig. 2. Relationship between 2.1SHya concentration and rOB cell adhesion after 24 h. rOB cells were treated with various concentrations of 2.1SHya. (A) Control. (B) 0.1 mg/ml of 2.1SHya. (C) 0.25 mg/ml of 2.1SHya. (D) 0.5 mg/ml of 2.1SHya. Phase contrast micrographs. Scale bar 200 μm.

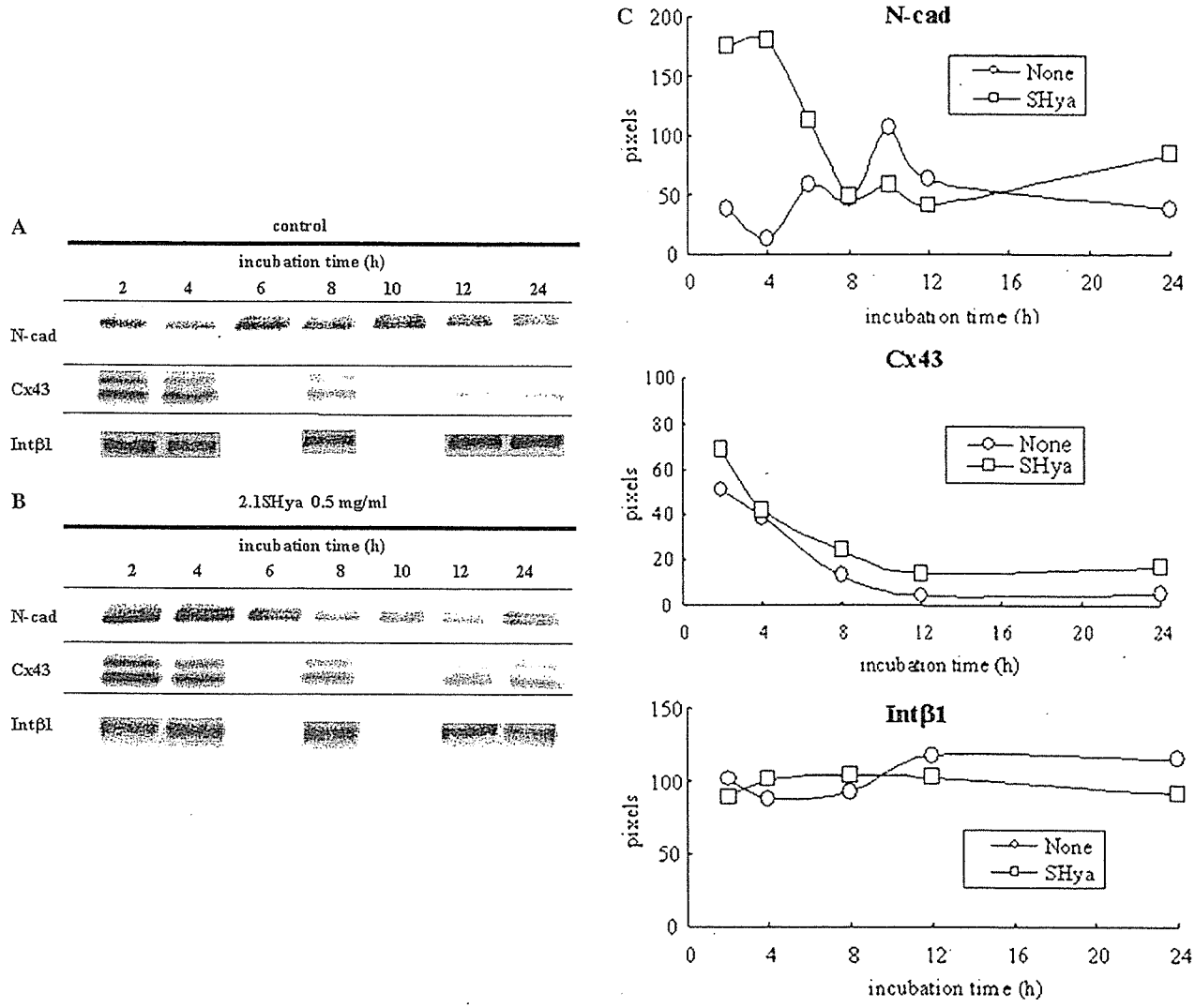

Fig. 3. Effect of SHya on adhesion protein expression in rOB cells. rOB cells were incubated with 2.1SHya for the times shown. Cells were lysed and proteins were separated by SDS–PAGE followed by Western blotting. (A) Without 2.1SHya (B) with 2.1SHya (C) quantification of band intensities was measured by NIH images.

was incubated in the culture medium including the serum (Fig. 8B) in comparison with the serum-free system. However, when SHya coexisted with the serum, rOB cells formed aggregations (Fig. 8C). rOB cells were seeded onto the plates in the presence or absence of FN and bFGF of added SHya for the study of effects of serum protein and SHya on cell aggregation (Fig. 9). bFGF was shown to form aggregation in rOB cells but not in the case of FN addition. Furthermore, when SHya was added with the bFGF, the cell aggregation was increased by the addition of SHya under the presence of bFGF.

Discussion

The aim of this study was to elucidate the mechanism of the enhancement of ALPase activity induced by the high molecular weight of sulfated polysaccharides. Hep, HS, and Hya are common components of the ECM in most tissues [19]. It is reported that sulfated polysaccharides like Hep/HS are the major FGF, TGF-β, and bone morphogenetic protein (BMP)-binding molecules in the ECM [20]. However, the molecular weights of Hep/HS and chondroitin sulfate (Chs) are lower than Hya [21]. Therefore, we synthesized SHya with varying DS and high molecular weight in order to obtain a high molecular weight of sulfated polysaccharides. Hya is easily decomposed in heat and acid [19]. Therefore, by the change of type and quantity of the SO_3 complex, SHya of varying DS and high molecular weight was synthesized. In this study, we examined the effect of SHya on the initial differentiation marker of the osteoblast. As a result of examining the effect of SHya in rOB cells on cell morphology, the following fact became clear: rOB cells formed aggregations in over 3 mg/ml

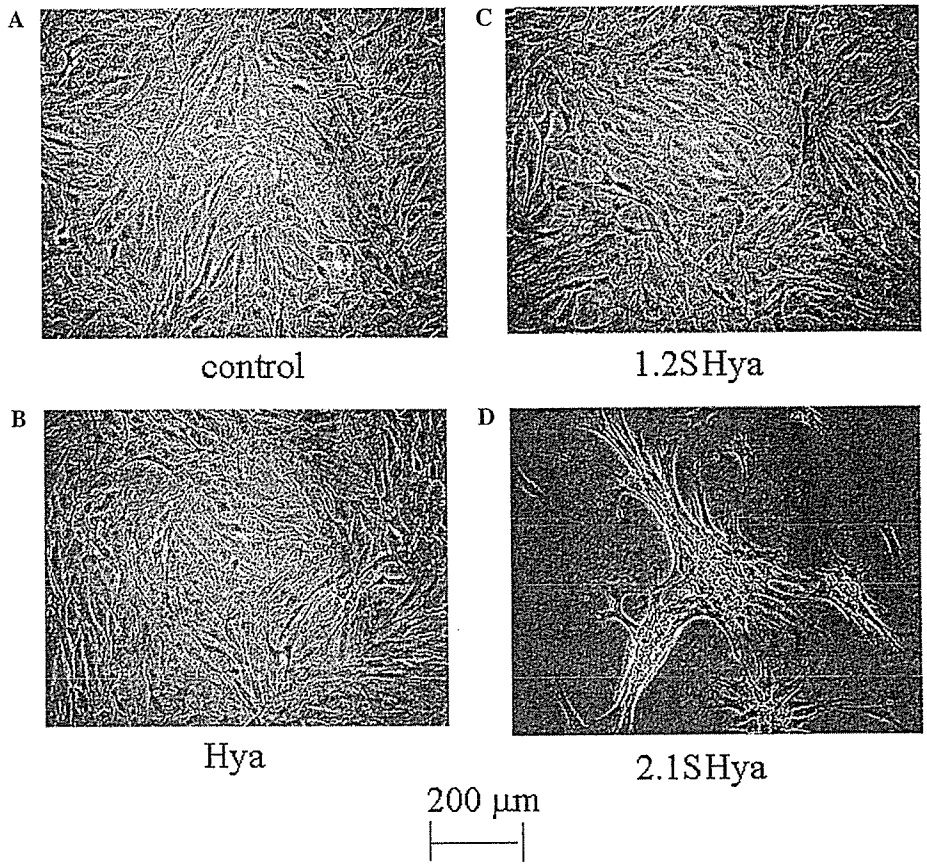

Fig. 4. Cell morphologies of rOB cells in the presence of 0.5 mg/ml Hya and SHya after 24 h. rOB cells were treated with Hya and varying DS of SHya. (A) Control, (B) Hya, (C) 1.2SHya, and (D) 3.4SHya.

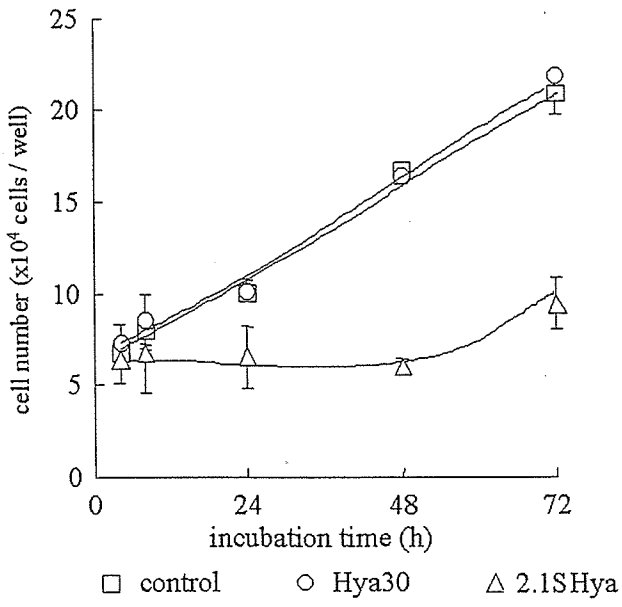

Fig. 5. Effect of 0.5 mg/ml Hya and SHya on the proliferation of rOB cells. rOB cells were treated with Hya and 2.1SHya for 72 h. The proliferation of rOB cells treated with Hya and 2.1SHya was determined. Values are means ± SD for four dishes.

concentration in the case of SHya of low DS (1.2SHya) and in over 0.25 mg/ml concentration in the case of SHya of high DS (2.1SHya, 3.4SHya). However, rOB cells cultured with Hya without the sulfate group did not form aggregations (data not shown). Also, aggregations were not formed when Hep and Chs were added. After the SHya addition, rOB cells began to form aggregations after 4 h and large aggregations were formed after 24 h. Therefore, by introducing a sulfate group into the hyaluronan, rOB cells formed aggregations.

Cell–cell contacts and communication between bone cells are essential for coordinated bone development and remodeling. Cell–cell adhesion mediated by the cadherin superfamily plays an important role in osteogenesis. Cadherins play essential roles in the regulation of several physiological processes such as cell migration, proliferation, and differentiation [22]. Tsutsumimoto et al. [23] reported that the expression of N-cad is involved in the aggregate formation of MC3T3-E1. Also, integrins are the principle mediators of the molecular dialogue between a cell and its ECM environment such as collagen and fibronectin [24,25]. Osteoblasts express several integrin subunits and their presence may be important in

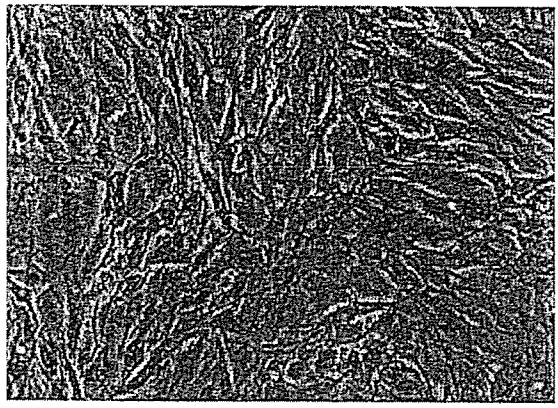

control

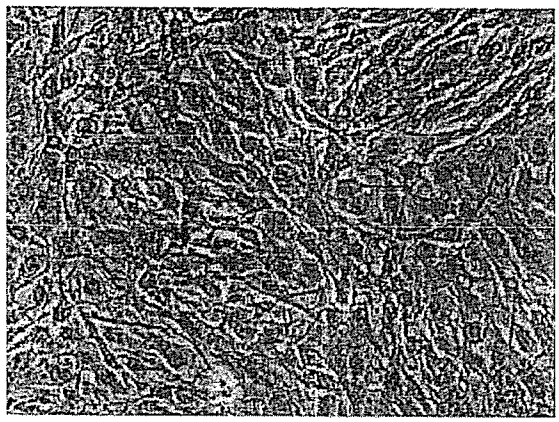

Hya

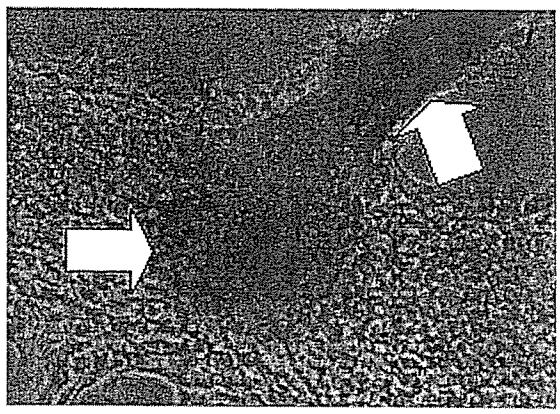

2.1SHya

Fig. 6. Appearance of Azo-stained cultures of rOB cells in the presence of 0.5 mg/ml Hya and SHya after 24 h. rOB cells were treated with Hya and 2.1SHya for 24 h. rOB cells were stained by the Azo stain method.

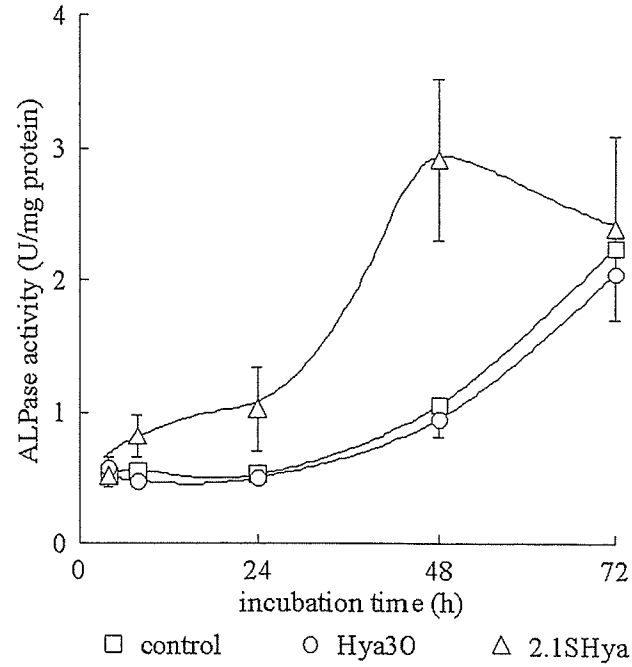

Fig. 7. Effect of 0.5 mg/ml Hya and SHya on the ALPase activity of rOB cells. rOB cells were treated with Hya and 2.1SHya for 72 h. The ALPase activity of rOB cells treated with Hya and 2.1SHya was determined. Values are means ± SD for four dishes.

regulating the response of these cells to the ECM, suggesting that integrin participates in the differentiation. By Western blotting, the expression of N-cad and Intβ1 proteins in osteoblasts was confirmed. In the presence of 2.1SHya, rOB cells increased protein levels of N-cad at early stages, but protein levels of Intβ1 were not observed in great difference between the 2.1SHya addition and control group. To clarify the roles of N-cad in SHya-induced cell aggregation, the effects of N-cad function-perturbing agents such as blocking antibodies were tested. This N-cad antibody was shown to inhibit cell–cell aggregation in rOB cells. These results confirm a direct involvement of N-cad in aggregation process (data not shown). Gap and adherens junctions are observed in osteoblast cell–cell contact [26,27]. Gap junctional intercellular communication (GJIC) is the key function by which cells exchange small molecules including signal molecules directly from the inside of a cell to neighboring cells. Gap junctions that are mediated by Cx have been well studied in osteoblasts. Among the Cx family, Cx43 is a major protein in osteoblasts [28]. By Western blotting, the expression of the Cx43 protein in these cells was confirmed. Cx43 expression level in the 2.1SHya addition reached a peak at 2–4 h, and the increase in expression level of protein was observed in comparison with the control. Some reports have proposed that cadherin is also involved in the regulation of the GJIC. This suggests that cadherin-mediated cell–cell adhesion is essential for GJIC and cadherin may also regulate GJIC in osteoblasts. Chiba et al. [29] demonstrated that Cx43 expression parallels ALPase activity and osteocalcin secretion in differentiating human osteoblastic cells. These data suggest that Cx43 expression contributes to osteoblastic differentiation.

Proliferation of rOB cells after aggregation formation was inhibited with the SHya addition more than with

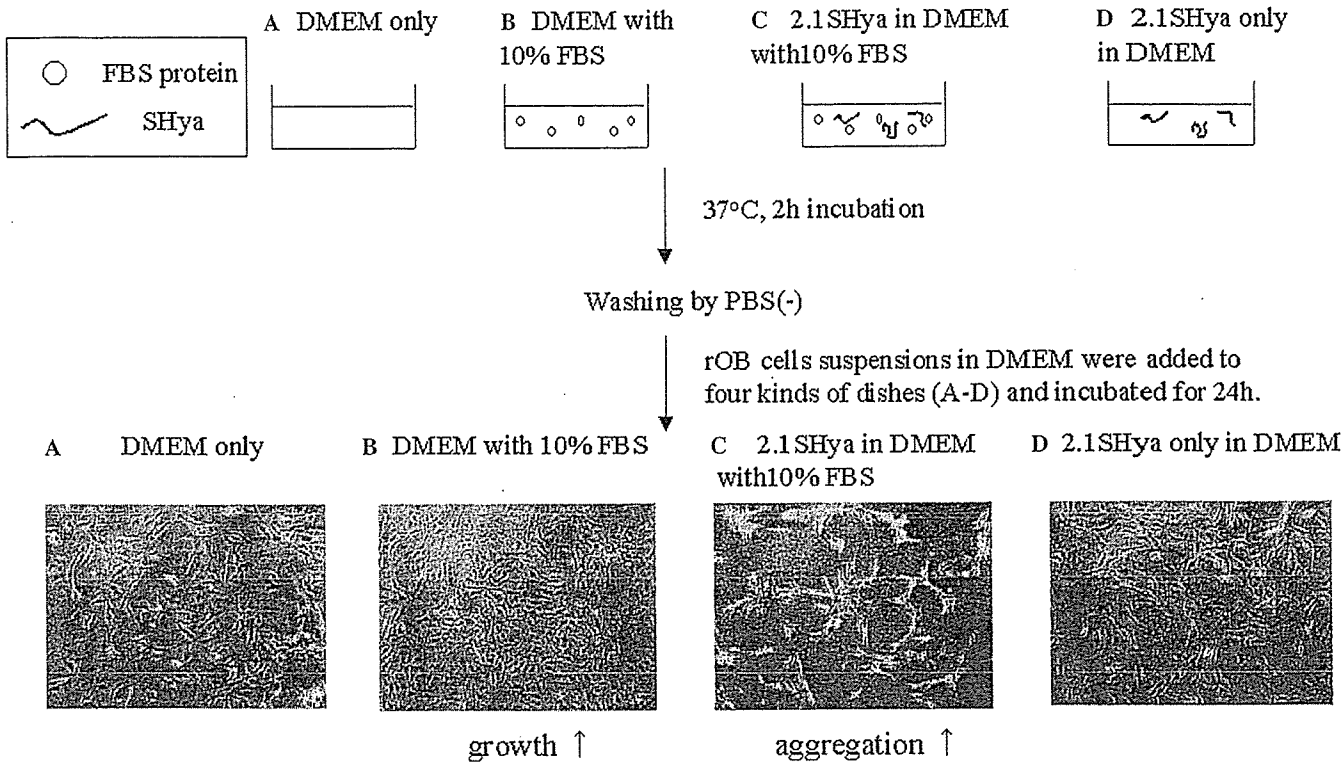

Fig. 8. Effect of FBS and 2.1SHya on cellular adhesion after 24 h. Four kinds of dishes were prepared as follows: (A) DMEM only, (B) DMEM with 10% FBS, (C) 2.1SHya in DMEM with 10% FBS, and (D) 2.1SHya only in DMEM into 35-mm tissue culture dish (NUNCLON) were incubated at 37 °C for 2 h under the 5% CO_2–95% air conditions, respectively, and washed with PBS (–) three times. Then, rOB cell suspensions in DMEM were added to four kinds of dishes (A–D). After 24 h-incubation, the cell appearances were observed as shown in (A–D). Magnification 100×.

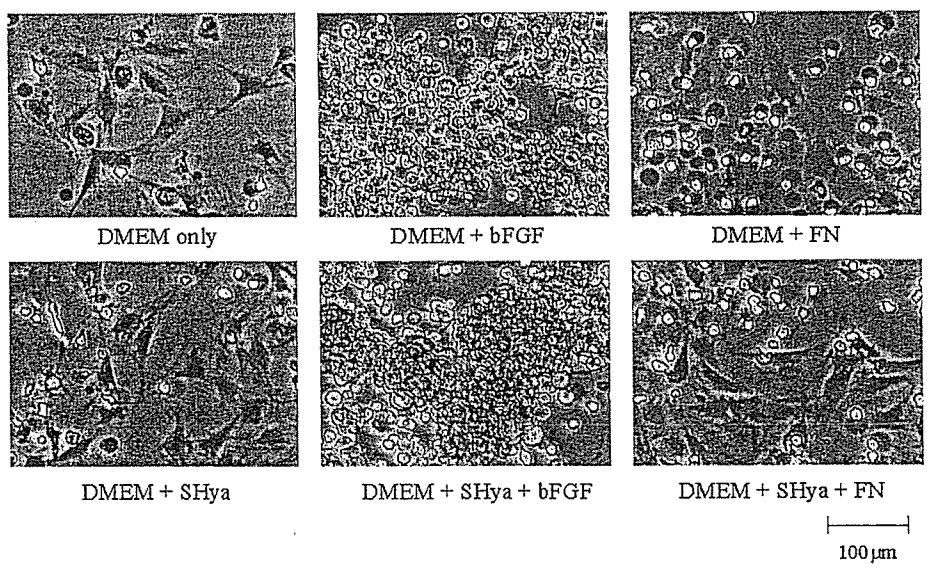

Fig. 9. Effect of serum component and 2.1SHya on cellular adhesion after 24 h. The cells were plated in serum free DMEM supplemented with FN, bFGF, and SHya, and incubated for 24 h at 37 °C with 5% CO_2.

the control or Hya addition. It is known that the osteoblast shifts to differentiation after it stops proliferation [30]. Recently, C-terminal Cx protein was found to suppress cell proliferation [31]. Then, we evaluated the effect of SHya on the ALPase activity of the initial differentiation marker for the osteoblast. The ALPase activity of rOB cells cultured with SHya was only expressed in the aggregation, when localization of the

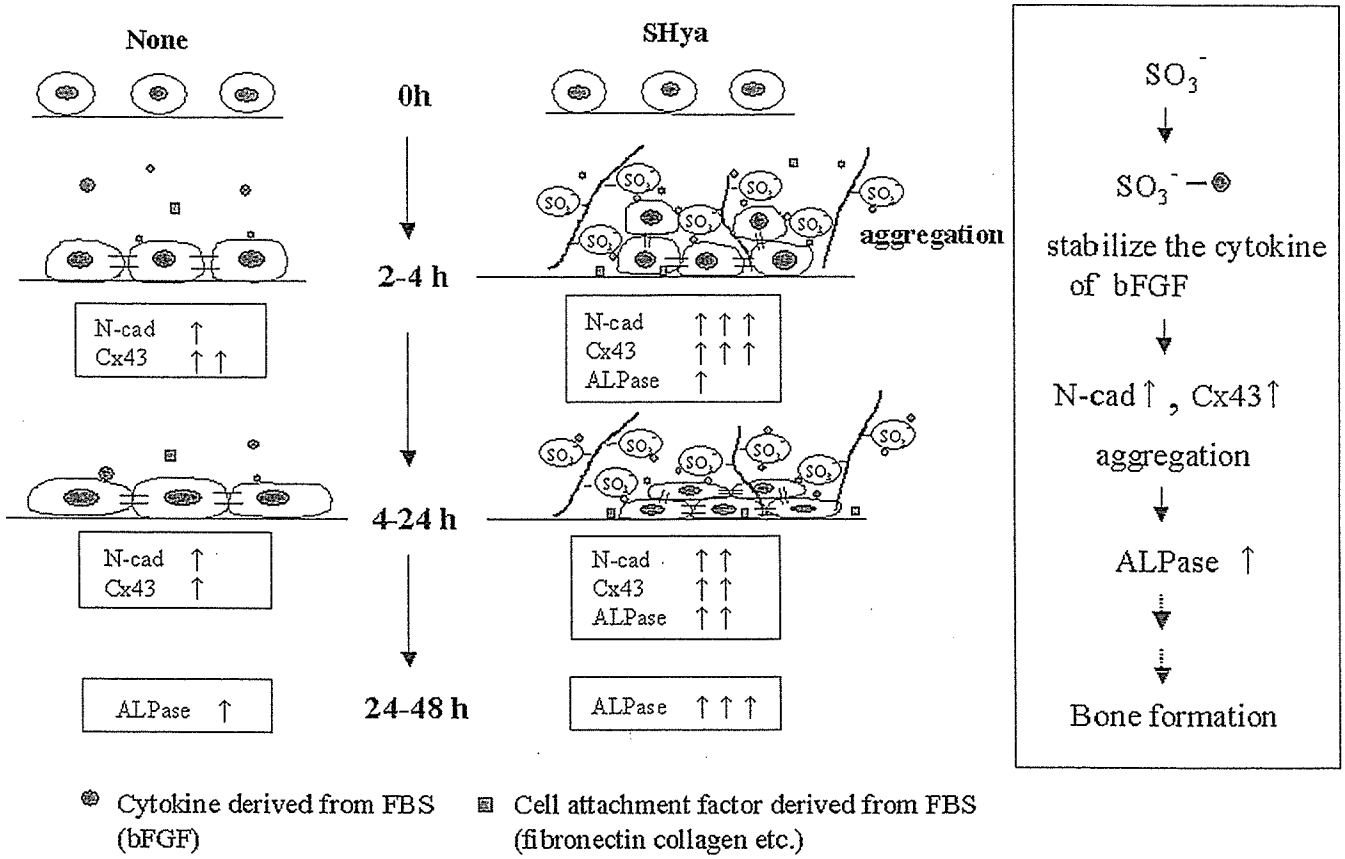

Fig. 10. SHya regulation of rat osteoblast cell differentiation.

ALPase activity was examined using the Azo staining method. The increased ratio and value of rOB cell ALPase activity with addition of SHya was higher than that of the control or Hya addition after 8 h. From the above results, the differentiation of rOB cells is promoted in aggregation, but the degree of proliferation is low as a whole. Therefore, it was shown that SHya controls rOB cell proliferation and differentiation, and that it especially promotes the differentiation. In this experiment, ALPase activity is enhanced while the expression of N-cad and Cx43 of rOB cells rises (Figs. 3, 6, and 7). Therefore, the expression of N-cad and Cx43 of rOB cells forming aggregations rises, and seems to promote the differentiation function, ALPase activity is enhanced with the aggregation formation of rOB cells.

In this experiment, 10% FBS was included in the culture medium. A serum of the usual 5–10% was included for the general culture medium used by the cell cultures of in vitro. The serum contained many components such as hormone, growth factor, cell adhesion molecule, and transportation protein [32]. Therefore, SHya interacted with the serum component, and it seemed to affect the cell. We examined the effect on the rOB cells by adding SHya to the serum-free medium. As the result, aggregations were not formed. However, when SHya coexisted with the serum, rOB cells formed aggregations. The interaction between the cell aggregation and the serum component such as FN, bFGF, and SHya was examined. In the case of FN, there was no effect on the cell aggregation. However, in the case of bFGF, cell aggregations were observed in both conditions with and without 2.1SHya. Therefore, it seems to relate the function of bFGF to the cell aggregation. N-cad expression of osteoblast by bFGF has been reported [22].

From these results, the effects of SHya on rOB cell function were not from the SHya alone; the data indicated that SHya affected rOB cell aggregation, proliferation, and differentiation by interacting with the serum component such as FGF and ECM (Fig. 10).

In conclusion, early expression of N-cad and Cx43 by SHya is the key to forming aggregations and enhancing the ALPase activity in rOB cells.

Acknowledgments

This work was partially supported by a Grant-in-Aid for the 21st Century COE Program and a Grant-in-Aid for Scientific Research (B) (14350495) by the Ministry of Education, Culture, Sports, Science and Technology, and Health and Labour Sciences Research Grants, Research on Advanced Medical Technology, Ministry of Health, Labour and Welfare, and Japan Health Sciences Foundation.

References

[1] J.C. Adams, F.M. Watt, Regulation of development and differentiation by the extracellular matrix, Development 117 (1993) 1183–1198.

[2] C.-H. Tang, R.-S. Yang, H.-C. Liou, W.-M. Fu, Enhancement of fibronectin synthesis and fiibrillogenesis by BMP-4 in cultured rat osteoblast, J. Bone Miner. Res. 18 (2003) 502–511.

[3] F. Blanuaert, D. Barritault, J.-P. Caruelle, Effects of heparin-like polymers associated with growth factors on osteoblast proliferation and phenotype expression, J. Biomed. Mater. Res. 44 (1999) 63–72.

[4] D.J. Baylink, R.D. Finkelman, S.E. Mohan, Growth factors to stimulate bone formation, J. Bone Miner. Res. 8 (1993) S565–S572.

[5] H. Ueda, L. Hong, M. Yamamoto, K. Shigeno, M. Inoue, T. Toba, M. Yoshitani, T. Nakamura, Y. Tabata, Y. Shimizu, Use of collagen sponge incorporating transforming growth factor-b1 to promote bone repair in skull defects in rabbits, Biomaterials 23 (2002) 1003–1010.

[6] A. Pilloni, G.W. Bernard, The effect of hyaluronan on mouse intramembranous osteogenesis in vitro, Cell Tissue Res. 294 (1998) 323–333.

[7] R. Barbucci, A. Magnani, M. Casoraro, N. Marchettini, C. Rosshi, M. Bosco, Modification of hyaluronic acid by insertion of sulphate groups to obtain a heparin-like molecule. Part I. Characterisation and behaviour in aqueous solution toward H^+ and Cu^{2+} ions, Gazzetta Chim. Italiana 125 (1995) 169–180.

[8] K. Nagasawa, H. Uchiyama, N. Wajima, Chemical sulfation of preparations of chondroitin4 and 6-sulfate, and dermatan sulfate preparation of chondroitin sulfate like materials from chondroitin4- sulfate, Charbohyd. Res. 158 (1986) 183–190.

[9] F. Dol, C. Caranobe, D. Dupony, M. Petitou, J.C. Lormeau, J. Choay, P. Sie, B. Boneu, Effects of increased sulfation of dermatan sulfate on its in vitro and in vivo pharmacological properties, Thrombosis Res. 52 (1988) 153–164.

[10] I. Yamamoto, K. Takayama, K. Honma, T. Gonda, K. Matsuzaki, K. Hatanaka, T. Uryu, O. Yoshida, H. Nakashima, N. Yamamoto, Y. Kaneko, T. Mimura, Synthesis, structure and antiviral activity of sulfates of cellulose and its branched derivatives, Carbohydr. Polymers 14 (1991) 53–63.

[11] R. Whistler, A.H. King, G. Ruffini, F.A. Lucas, Sulfation of cellulose with sulfur trioxide–dimethyl sulfoxide, Arch. Biochem. Biophys. 121 (1967) 358–363.

[12] R.L. Whistler, D.G. Unrau, G. Ruffini, Preparation and properties of a new series of starch sulfates, Arch. Biochem. Biophys. 126 (1968) 647–652.

[13] C.T. Wright, M. Petitou, Structural determinants of heparin's growth inhibitory activity, J. Biol. Chem. 264 (1989) 1534–1542.

[14] T. Hamano, H. Suzuki, A. Teramoto, E. Iizuka, K. Abe, Functional culture of human periodontal ligament fibroblast (HPLF) on polyelectrolyte complex (PEC), J. Macromol. Sci. Chem. A 35 (2) (1998) 439–455.

[15] G. Anderegg, H. Flaschka, R. Sallmann, G. Schwarzenbach, Metallindikatoren VII. Ein auf Erdalkaliionen ansprechendes Phatalein und sein analytische Verwendung, Helv. Chim. Acta 37 (1954) 113–120.

[16] T. Hamano, D. Chiba, K. Nakatsuka, M. Nagahata, A. Teramoto, Y. Kondo, A. Hachimori, K. Abe, Evalution of a polyelectrolyte complex (PEC) composed of chitin derivatives and chitosan, which promotes the rat calvarial osteoblast differentiation, Polym. Adv. Technol. 13 (2002) 46–53.

[17] N. Matsuda, M. Horikawa, L.-H. Wang, M. Yoshida, K. Okaichi, Y. Okumura, M. Watanabe, Differntial activation of ERK 1/2 and JNK in normal human fibroblast-like cells in response to UVC radiation under different oxygen tensions, Photochem. Photobiol. 72 (2000) 334–339.

[18] O.H. Lowry, N.R. Roberts, M.-L. Wu, W.S. Hixon, E.J. Crawford, The quantitative histochemistry of brain. II. enzyme measurements, J. Biol. Chem. 207 (1954) 19–37.

[19] L.S. Liu, C.K. Ng, A.Y. Thompson, J.W. Poser, R.C. Spiro, Hyaluronate–heparin conjugate gels for the delivery of basic fibroblast growth factor (FGF-2), J. Biomed. Mater. Res. 62 (2002) 128–135.

[20] A. Walker, J.E. Turnbull, J.T. Gallagher, Specific heparan sulfate saccharides mediate the activity of basic fibroblast growth factor, J. Biol. Chem. 269 (1994) 931–935.

[21] H.B. Nader, T.M. Ferreira, J.F. Paiva, M.G. Medeiros, S.M. Jeronimo, V.M. Paiva, C.P. Dietrich, Isolation and structural studies of heparan sulfates and chondroitin sulfates from three species of mollusks, J. Biol. Chem. 259 (1984) 1431–1435.

[22] P.J. Marie, Role of N-cadherin in bone formation, J. Cell. Physiol. 190 (2002) 297–305.

[23] T. Tsutsumimoto, S. Kawasaki, S. Ebara, K. Takaoka, TNF-a and IL-1b suppress N-cadherin expression in MC3T3-E1 cells, J. Bone Miner. Res. 14 (1999) 1751–1760.

[24] E.A. Clark, J.S. Brugger, Integrins and signal transduction pathways: the road taken, Science 268 (1995) 233–239.

[25] Y. Takeuchi, M. Suzawa, T. Kikuchi, E. Nishida, T. Fujita, T. Matsumoto, Differentiation and transforming growth factor-receptor down-regulation by collagen-21 integrin interaction is mediated by focal adhesion kinase and its downstream signals in murine osteoblastic cells, J. Biol. Chem. 272 (1997) 29309–29316.

[26] Z. Li, Z. Zhou, C.E. Yellowley, H.J. Donahue, Inhibiting gap junctional intercellular communication alter expression of differentiation markers in osteoblastic cells, Bone 25 (1999) 661–666.

[27] H.J. Donahue, Z. Li, Z. Zhou, C.E. Yellowley, Differentiation of human fetal osteoblastic cells, Am. J. Physiol. Cell. Physiol. 278 (2000) 315–322.

[28] P.C. Shiller, G. D'ippolito, W. Balkan, B.R. Roos, G.A. Howard, Gap-junctional communication is required for the maturation process of osteoblastic cells in culture, Bone 28 (2001) 362–369.

[29] H. Chiba, N. Sawada, M. Oyamada, T. Kojima, S. Nomura, S. Ishii, M. Mori, Relationship between the expression of the gap junction protein and osteoblast phenotype in a human osteoblastic cell line during cell proliferation, Cell Struct. Funct. 18 (1993) 419–426.

[30] C.G. Bellows, J.E. Aubin, J.N. Heerche, M.E. Antosz, Mineralized bone nodules formed in vitro from enzymatically released rat calvaria cell populations, Calcif. Tissue Int. 38 (1986) 143–154.

[31] C. Moorby, M. Patel, Dual functions for connexins: Cx43 regulates growth independently of gap junction formation, Exp. Cell Res. 271 (2001) 238–248.

[32] A.L. Koenig, V. Gambillara, D.W. Grainger, Correlating fibronectin adsorption with endothelial cell adhesion and signaling on polymer substrates, J. Biomed. Mater. Res. 64A (2003) 20–37.

Available online at www.sciencedirect.com

SCIENCE DIRECT

European Journal of Pharmacology 495 (2004) 27–33

ejp

www.elsevier.com/locate/ejphar

Desensitization of $P2X_2$ receptor/channel pore mutants

Ken Nakazawa[a,b,*], Yasuo Ohno[b]

[a] *Molecular and Cellular Pharmacology Section, National Institute of Health Sciences, 1-18-1 Kamiyoga, Setagaya, Tokyo 158-8501, Japan*
[b] *Division of Pharmacology, National Institute of Health Sciences, 1-18-1 Kamiyoga, Setagaya, Tokyo 158-8501, Japan*

Received 8 January 2004; received in revised form 10 May 2004; accepted 12 May 2004

Abstract

Properties of five mutants of $P2X_2$ receptor/channel having amino acid residue-substitution at the pore region were examined by expressing the channels in *Xenopus* oocytes. When the concentration–response relationship for ATP-evoked current was obtained, the current amplitude was increased along with the concentrations of ATP for the wild type channel whereas the amplitude was rather decreased with highest concentrations for four of the five mutants as if an "inactivation-like" mechanism occurs to these mutants. Upon a long exposure (30 s) to ATP, time-dependent decay in the ATP-evoked current was observed for three of the five mutants, suggesting that desensitization occurs to these mutants. The time course of the desensitization was well fitted with a single exponential time whereas that of the recovery from the desensitization could be better fitted with multiple exponentials than with a single exponential. The relationship between the desensitization and the "inactivation-like" mechanism was discussed.

Keywords: $P2X_2$ receptor; Channel pore mutant; Desensitization; ATP responsiveness

1. Introduction

When appropriate stimulation (change in membrane potential or ligand-binding) is given, voltage- and ligand-gated ion channels, respectively, exhibit transition from closed state to open state. In a number of channels, opened channels gradually shut even if the stimulation continues. This phenomenon is called "inactivation" for voltage-gated channels (Hodgkin and Huxley, 1952; Hille, 1992a), and generally called "desensitization" for ligand-gated channels (Katz and Thesleff, 1957; Hille, 1992b). The desensitization was also found for ion channels gated by extracellular ATP (P2X receptor/channels; see reviews, Ralevic and Burnstock, 1998; Khakh, 2001; North, 2002). Among P2X receptor/channel subclasses, $P2X_1$ and $P2X_3$ receptor/channels exhibit marked desensitization whereas the $P2X_2$ receptor/channel does not exhibit desensitization when expressed as homomeric channels.

We previously utilized channel pore mutants of $P2X_2$ receptors to determine factors contributing to the potency of multivalent cation block (Nakazawa et al., 2002). In the present study, we studied the dependence of the current permeating through these pore mutants on ATP concentrations, and the kinetics of the current during a long exposure to ATP. We found an "inactivation-like" phenomenon in the concentration–response study and desensitization in the kinetic study. The time courses of the desensitization and recovery from the desensitization were analyzed, and the relation between the desensitization and the "inactivation-like phenomenon was discussed using possible schematic models.

2. Materials and methods

2.1. Ionic current measurement

Mutants of $P2X_2$ receptor constructed from the cloned rat $P2X_2$ receptor (Brake et al., 1994) used in this study were those described by Nakazawa et al. (2002). The substitutions applied to the mutants were Asn^{333} to alanine (N333A), Thr^{336} to alanine (T336A), Leu^{338} to alanine (L338A), Gly^{342} to alanine (G342A) and Asp^{349} to asparagine (D349N). Channels were expressed in *Xenopus* oocytes and ionic currents permeating through them were measured

* Corresponding author. Tel.: +81-3-3700-9704; fax: +81-3-3707-6950.
E-mail address: nakazawa@nihs.go.jp (K. Nakazawa).

0014-2999/$ - see front matter © 2004 Elsevier B.V. All rights reserved.
doi:10.1016/j.ejphar.2004.05.021

as previously described (Nakazawa and Ohno, 1996; Nakazawa et al., 1998). Oocytes were bathed in ND96 solution containing (in mM) NaCl 96, KCl 2, $CaCl_2$ 1.8, $MgCl_2$ 1, HEPES 5 (pH 7.5 with NaOH) at room temperature. For the construction of concentration–response curves, ATP (adenosine 5′ -triphosphate disodium salt; Sigma, St. Louis, MO, USA) was applied by superfusion for 7 s with a regular interval of 1 min from the lowest concentration (usually 30 μM). To determine desensitization time course, ATP was applied for 30 s. For the determination of the time course of recovery from desensitization, reference responses to ATP were measured with an interval of 4 min, and trials were made with various intervals.

2.2. Data analysis

All the data were given as mean ± S.E. Curve fittings to data were made using Microsoft' Excel X. For "activation" of channels (see Fig. 2), curves were calculated from the following equation (Tallarida and Jacob, 1979):

$$E = E_{max} \cdot A^n / [A^n + (EC_{50})^n] \quad (1)$$

where E is an effect (current response), E_{max} is an maximal response, A is ATP concentration, EC_{50} is concentration required for a half-maximal effect, and n is a Hill coefficient (slope factor). As for "inactivation" curves, the following equation was used:

$$E = E_{max} \cdot (1 - A^n / [A^n + (EC_{50})^n]). \quad (2)$$

Curve fittings to the recovery from desensitization (Fig. 5) were made with an assumption of the following Hodgkin–Huxley type gating mechanism (Hille, 1992a):

$$I = m^k \cdot I_{max} \quad (3)$$

where I is current activated by ATP, I_{max} is its maximal value, k is the number of gates, and m is a gate variable given by:

$$m = 1 - \exp(-t/\tau) \quad (4)$$

where τ is a time constant.

3. Results

3.1. Concentration–response relationship

Fig. 1 shows concentration–response relationships for ATP-activated current permeating through the wild type and pore mutant $P2X_2$ receptor/channels. For the pore mutants, alanine-substituted ones were used except for D349N because D349A was an non-expressing mutant. Compared to the wild type channel, N333A and D349N exhibited higher sensitivities to ATP. Unlike the wild type channel, current responses to ATP were rather reduced at highest concentrations (300 μM, 1 mM or 3 mM) for N333A, T336A, L338A and D349N. To analyze these properties quantitatively, we plotted the relationships separately, and curve fittings were made (Fig. 2). Modeling after the gating theory for voltage-gated channels (Hodgkin and Huxley, 1952; Hille, 1992a), "activation" and "inactivation" curves were fitted to the data as described in Materials and methods. All the curves were well fitted to the data when assuming a common Hill coefficient of 2. For "activation", EC_{50} values for N333A (50 μM) and D349N (60 μM) were smaller than that for the wild type receptor (100 μM). On the other hand, a larger EC_{50} value (180 μM) was necessary for L338A activation fitting. As for "inactivation", the decease of the current responses to higher concentrations of ATP could be fitted with curves with EC_{50} values of millimolar for N333A, T336A, L338A and D349N. The results imply that the decrease can be explained if assuming that higher concentrations of ATP shut an "inactivation" gate.

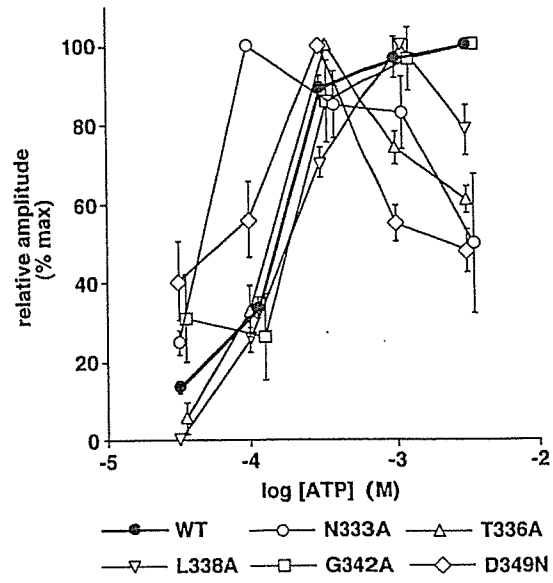

Fig. 1. Concentration–response relationships for ionic current activated by ATP permeating through the wild type (WT) and five pore mutant (N333A, T336A, L338A, G342A and D349N) channels. A current response to each concentration of ATP at − 50 mV was normalized to the maximal response in each oocyte. Each symbol represents the mean obtained four to six oocytes tested. Bars are S.E.

3.2. Desensitization time course

Fig. 3 compares time course of inward current activated by ATP for 30 s. The current permeating through the wild type channel sustained during a 30-s exposure to 1 mM ATP (Fig. 3A) whereas that through D349N markedly decayed (Fig. 3B). The results indicate that desensitization occur to D349N but not to the wild type channel. The current remaining at the end of the 30-s exposure to 100 μM or 1 mM ATP was plotted in Fig. 3C. Marked desensitization was observed with the current permeating through N333A and G342A as well as D349N. The extent of

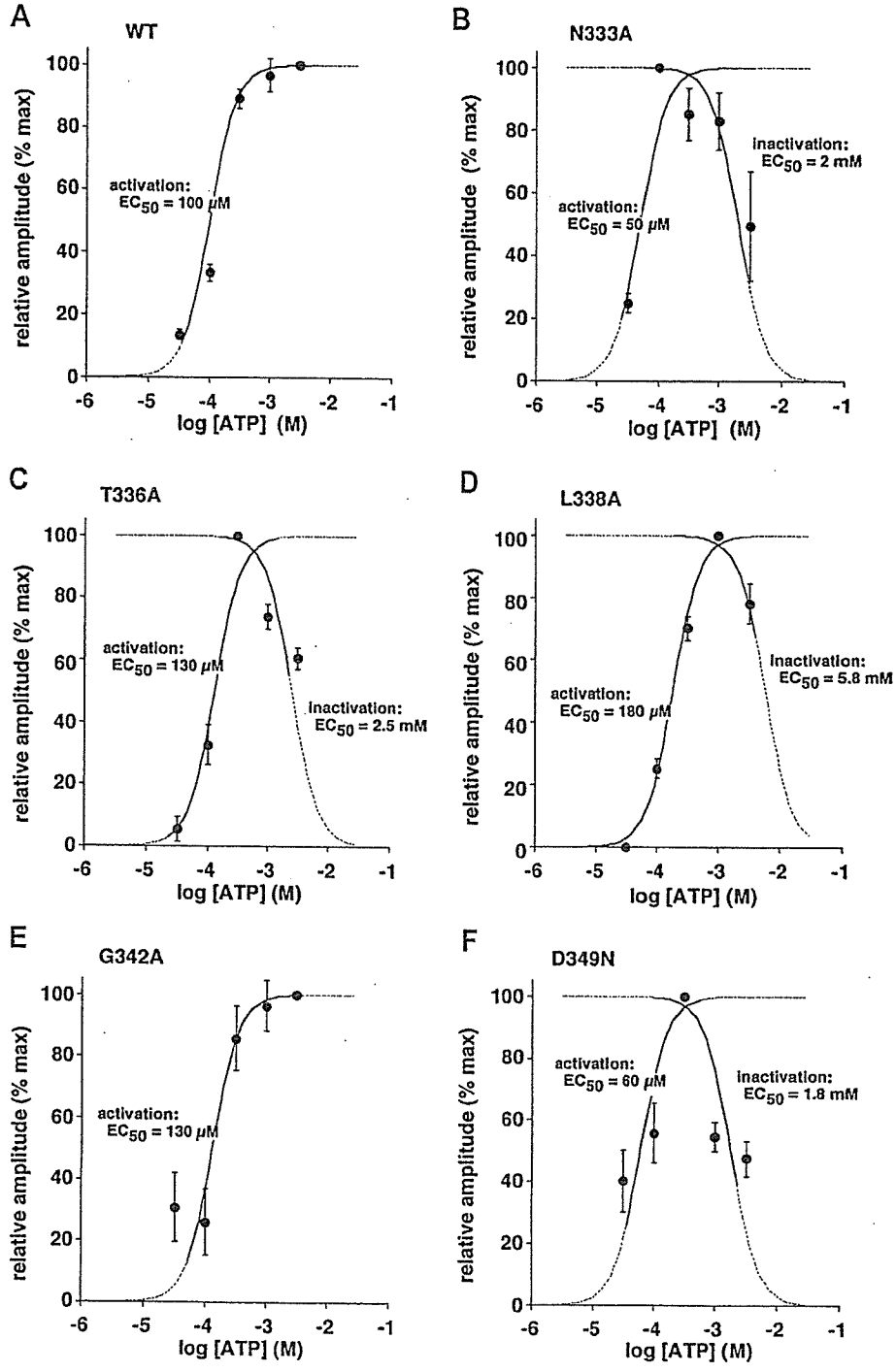

Fig. 2. Curve-fittings to concentration–response data for the ATP-activated current. "Activation" and "inactivation" curves were fitted to the data shown in Fig. 1 assuming a Hill coefficient of 2 and EC_{50} values shown in panels A to F.

desensitization was not different between the current activated by 100 μM ATP and that by 1 mM ATP for each mutant when the remaining current amplitude was compared (Fig. 3C). The current activated by a lower concentration (30 μM) of ATP was not desensitized up to 1 min for D349N (not shown).

The current amplitude remaining at the end of the 30-s exposure does not necessarily reflect desensitization time course because this value may be affected by other factors such as activation kinetics or multiple components of desenstization. Thus, the time course was further analyzed by measuring time constants. The oocytes were periodically stepped to −80 from −50 mV to obtain large current amplitude and to confirm clamp conditions of oocytes. For the current mediated through D349N shown in Fig. 3B, the decay could be fitted by a single

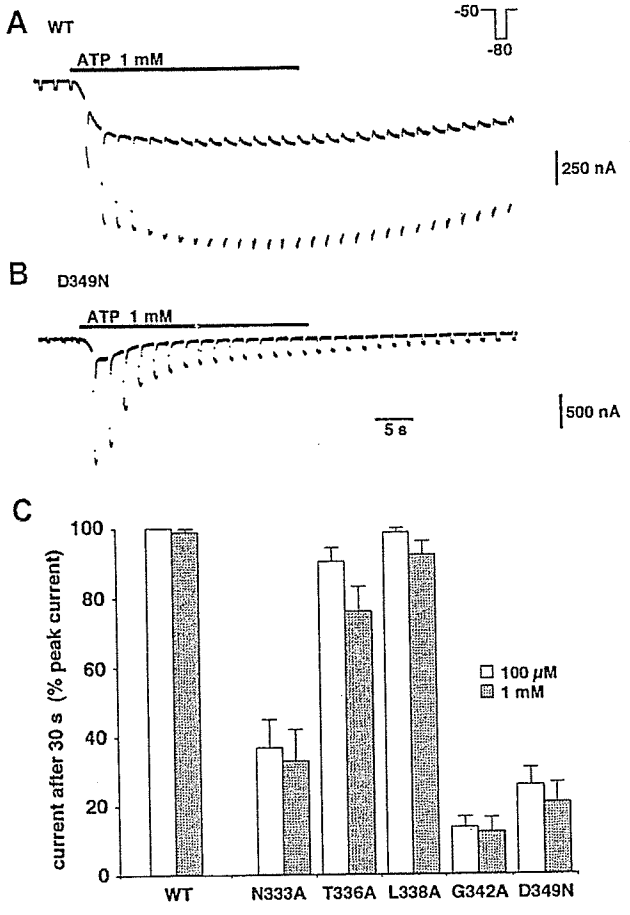

Fig. 3. Desensitization of ATP-activated current. (A, B) Comparison of time courses of ATP-activated current permeating through the wild type (WT; A) and D349N mutant (B) channels. ATP (1 mM) was applied for 30 s. The oocytes were held at −50 mV and stepped to −80 mV for 400 ms every 2 s. Note that the current through the wild type channel (A) was not desensitized whereas that through D349N mutant channel (B) was desensitized. (C) Comparison of the extent of desensitization. The current remaining at the end of 30 s application of 100 μM or 1 mM ATP was normalized to the peak amplitude, and plotted for the wild type (WT) and five pore mutant channels. Each column represents the mean obtained from five to seven oocytes tested. Bars are S.E.

exponential time course with a time constant of 5 s (Fig. 4A). Time constants obtained in this manner were compared in Fig. 4B. Like the current amplitude remaining at the end of the ATP exposure (Fig. 3C), the time constants were not different between the currents activated by 100 μM and 1 mM ATP for N333A and D349N. With G342A, the time constants for the current activated by 1 mM ATP were, however, smaller than that by 100 μM ATP.

3.3. Recovery from desensitization

Once desensitized, the current was not readily restored. After a 2-min washout period, the current permeating through D349N was recovered to about a half of the initial level (Fig. 5A). Fig. 5B and C shows the time course of recovery from desensitization of the currents through N333A and D349N. For both mutants, the currents were recovered to about initial levels after a 4-min washout period. For G342A, the current was recovered only to 36.1 ± 11.6% of the initial level after 4 min.

Curve fittings were made for time courses of the recovery from desensitization using the Eqs. (3) and (4) in Materials and methods. When a single "recovery" gate is assumed, the current amplitude after short washout periods (1 and 2 min) was poorly fitted by curves adjusted to fit to the current amplitude after a 4-min washout period (Fig. 5B and C; $k=1$). This means that the initial recovery was slower than that expected from this single gate model. The fittings became better when multiple "recovery" gates are assumed (Fig. 5B and C;

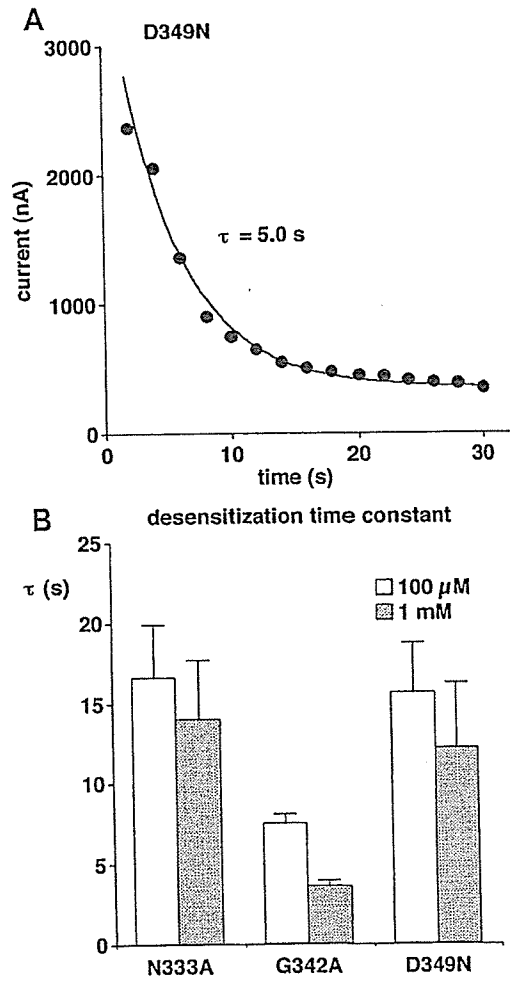

Fig. 4. Desensitization time constants. (A) A curve-fitting to the desensitization time course of ATP-activated current permeating through D349 mutant channel. The data were obtained from the current trace shown in Fig. 3B. The current amplitude at −80 mV was plotted against the time after the beginning of the ATP-application. The data were well fitted with a single exponential time course with a time constant of 5.0 s. (B) Desensitization time constants for three pore mutants. The time constants were obtained as illustrated in A. Each column represents the mean obtained from five to seven oocytes tested. Bars are S.E.

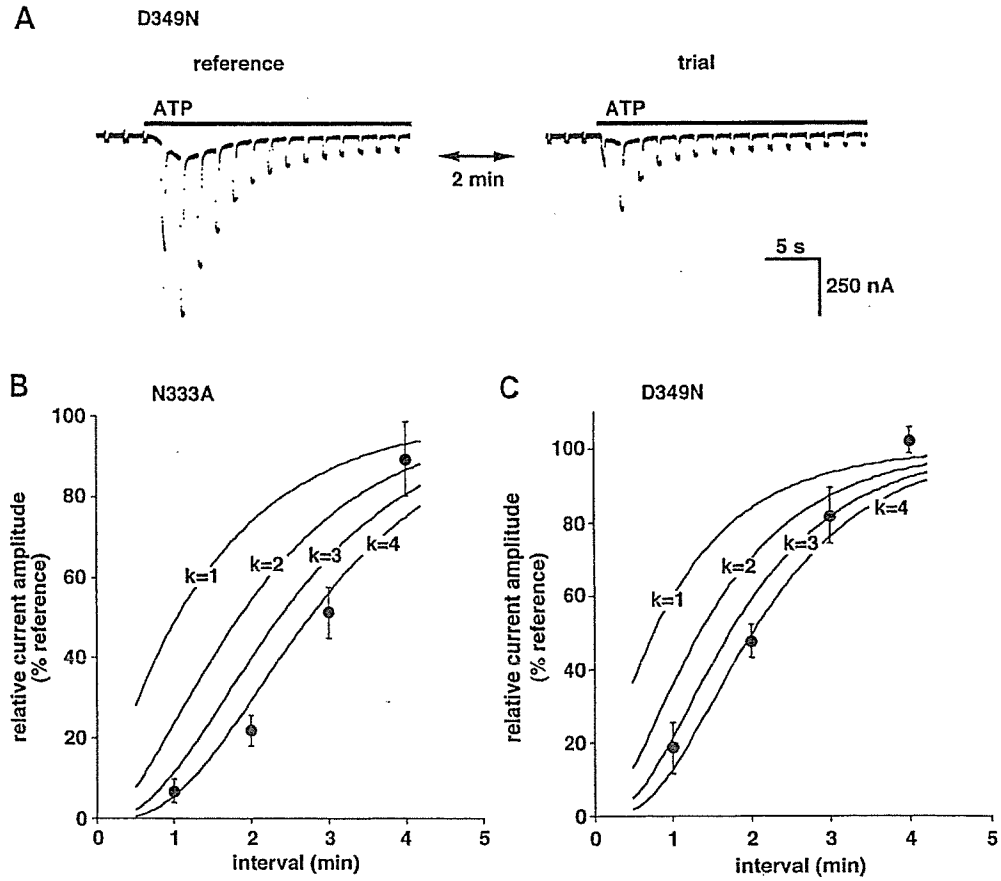

Fig. 5. Recovery from desensitization. (A) Current responses to two sequential 30-s applications of 1 mM ATP with an interval of 2 min in a D349N expressing oocyte. The response to the second application (trial) was about 40% of that to the first application (reference) in this case. (B) Time courses of recovery from desensitization of the current permeating through N333A (B) and D349N (C). Each symbol represents the mean from six oocytes tested. Bars are S.E.M. Three curves in each panel are curve-fittings with assumption of one, two, three and four homogeneous gates with a time constant of 1.5 min (N333A) or 1.1 min (D349N), respectively.

$k=2$, 3 and 4) because these multiple gate models allow slower initial recovery.

4. Discussion

In the present study, we first analyzed the "inactivation-like" property observed in the concentration–response relationship for the mutants of $P2X_2$ receptor/channel, and then analyzed the desensitization process of the mutants to compare the desensitization with the "inactivation". The mutants used in the present study possess amino acid substitutions at TM2 region of $P2X_2$ receptor/channel. This region contributes to the forming of the channel pore, and N333, T336, L338, G342 and D349 face the aqueous phase in the pore (Rassendren et al., 1997; Egan et al., 1998). The binding-site for ATP molecules are believed to be somewhere in the extracellular region of P2X receptor involving basic residues near the outer mouth of the channel pore (Ennion et al., 2000; Jiang et al., 2000). Thus, the changes in sensitivity to ATP (Fig. 1) or kinetics (Fig. 3) may not be due to direct influence by the amino acid substitutions of ATP binding, but due to some allosteric influence.

N333A, T336A, L338A and D349N exhibited reduced responses to higher concentrations of ATP (Fig. 2). These "downward limbs" could be fitted with "inactivation" curves with EC_{50} values of millimolar order. This fact may not imply the appearance of a second low-affinity binding-site on receptor subunits with these mutations. Rather, this fact may imply that the induction of this "inactivation-like" site requires higher energy than that necessary for the open state, and, thus, larger occupation by ATP molecules of the receptors is necessary. This is explained by the following simple sequential scheme (Tallarida and Jacob, 1979): where R is a receptor and A is an

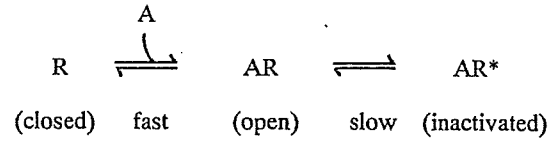

Scheme 1.

agonist (ATP). In this scheme, only one ATP molecule and one receptor subunit are shown for simplicity. The number of inactivated receptors (AR*) is negligible when the concentration of ATP is low. The number of AR* becomes considerable only when the concentration of ATP is high and as, a result, the number of AR is large.

If the process toward the inactivated state in Scheme 1 is slow enough, the current amplitude does not readily reach its steady-state, and this process will be observed as a current decay during a long exposure to ATP. In fact, the currents permeating through N333A and D349N, which exhibited "inactivation" in the concentration–response relationships (Fig. 2B and F), decayed during a 30-s exposure to high concentrations of ATP (Fig. 3B, C) whereas the current through the wild type channel did not exhibit such decay (Fig. 3A, C). However, this is not the case with the remaining pore mutants, T336A, L338A and G342A. T336A and L338A exhibited "inactivation" in the concentration–response relationships (Fig. 2C and D), but the current permeating through these mutants did not remarkably decay (Fig. 3C). As for G342A, the "inactivation" was not observed in the concentration–response relationship (Fig. 2E), the current through this mutant markedly decayed (Fig. 2C). The discrepancy may be explained if another "desensitized" state is added to the Scheme 1: (Scheme 2).

According to this scheme, "inactivation" and "desensitization" are independent processes. The transition to the inactivated state (AR*) is slow but faster than the transition to the desensitized state (AR**). AR and AR* readily reach their equilibrium, and the portion of the inactivated channels is observed as a reduction in peak amplitude, but not as a decay in current amplitude with time. In contrast, AR and

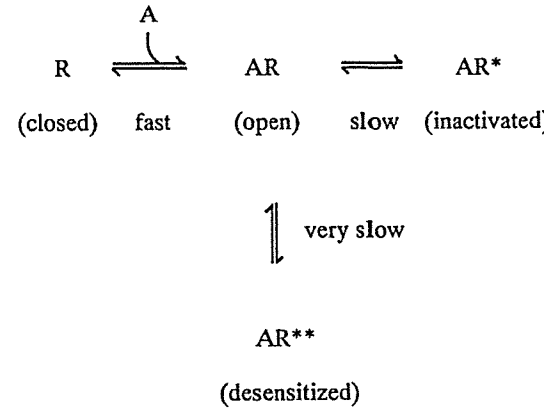

Scheme 2.

AR** do not readily reach their equilibrium, and the transition to AR** is observed mainly as a current decay with time after peak current. The transition to AR** may be slower enough for the current decay to be independent of agonist concentrations (Fig. 3). N333A and D349N can shift into both AR* and AR**, T336A and L338A can shift mainly into AR*, G342A can shift only into AR**, and the wild type channel can shift into neither AR* nor AR**. Further study will be necessary whether or not the proposed two states can be defined as molecular conformations of the receptor.

The desensitization time course of N333A, G342A and D349N could be fitted by a single exponential (Fig. 4). This suggests that the closing of a single gate is sufficient to induce the desensitization. On the other hand, the time course of the recovery from the desensitization was not well fitted by a single exponential, and the introduction of multiple exponentials resulted in better fittings to the data

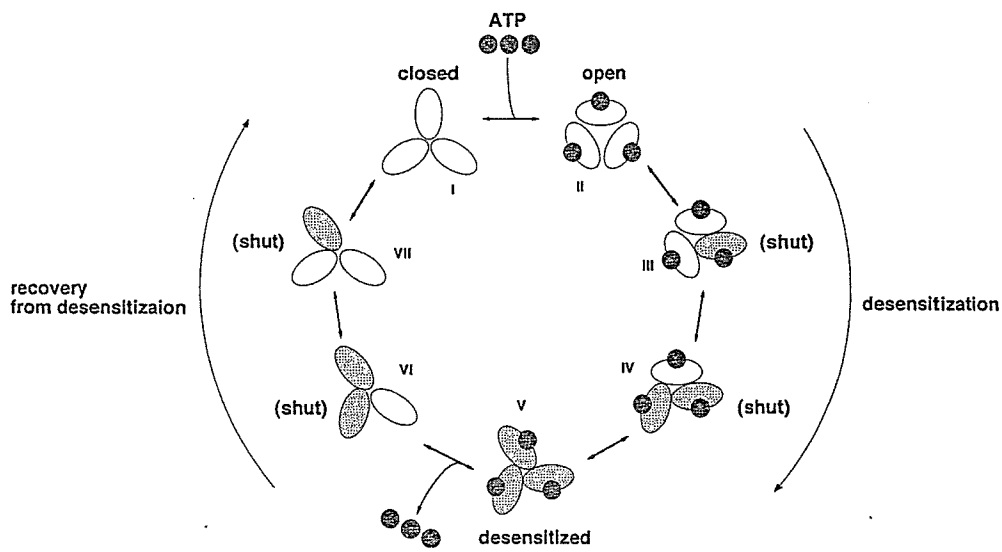

Fig. 6. A schematic model for desensitization and the recovery from desensitization of $P2X_2$ receptor pore mutants. One channel consists of three homogenous subunits. A closed channel (I) is open when ATP molecules bind (II). The open channel is shut when one of the three subunits is shifted to its "desensitized" conformation (III). As for the recovery from desensitization, the desensitized channel (V) is shut until all the subunit is shifted from the "desensitized" conformation (I; closed state).

(Fig. 5). The requirement of multiple exponentials implies that more than one gate should be "on" before the opening of the channel. Based on the trimeric composition of P2X receptors (Nicke et al., 1998; Stoop et al., 1999), these gating mechanisms can schematically explained as shown in Fig. 6. A trimeric $P2X_2$ receptor/channel opens upon the binding of ATP molecules (from state I to state II). The open channel then slowly shifts to the desensitized state. In this process, three subunits independently change their conformations (states III, IV and V), and the channel is shut when one of the subunits has changed its conformation (state III). Thus, the desensitization progresses in the first order kinetics. As for the recovery from the desensitization, the subunits also independently change their conformations (states VI, VII and I), but the channel cannot open until all the subunits have changed the conformations (state I). Thus, the recovery process follows multiple order kinetics.

Although the model shown in Fig. 6 is one of possible explanations, the recovery from the desensitization may, in any case, involves some very slow (in minutes) mechanisms. In rat superior cervical ganglia, $P2X_1$ receptors disappear from cell surface within 1 min after stimulation by agonists, and they are redistributed in the order of minutes at room temperature (Li et al., 2000). Similar redistribution of $P2X_2$ receptors has also been reported in rat hippocampal neurons, and this phenomenon occurs faster (5–10 s) at 32–34 °C (Khakh et al., 2001). The latter appears to require protein kinase C because the phenomenon was not observed when the phosphorylation site was blocked by mutagenesis (T18A). Interestingly, the current permeating through T18A also decays (Khakh et al., 2001) because of its inability to shift to the "second" open state, which appears with the phosphorylated wild type channel during a long exposure to ATP. The relationship of this current decay in T18A and the desensitization of the pore mutants observed in the present study remains to be clarified.

Neither desensitization nor the "inactivation-like" phenomenon was observed with the wild type $P2X_2$ receptor. This implies that the channel pore of the wild type receptor is elaborate enough to escape from these shutting mechanisms. Alternatively, native desensitizing P2X subclasses, such as $P2X_1$ or $P2X_3$, may possess pore structures suitable for desensitization. This view may be favored by the finding that desensitization of chimeric channels constructed from $P2X_1$ and $P2X_2$ are determined by pore forming regions (Werner et al., 1996).

Acknowledgements

We are grateful to H. Sawa for the participation in a part of experiments. This work was partly supported by a Health and Labour Science Research Grant for Research on Advanced Medical Technology from the Ministry of Health, Labour and Welfare, Japan, and a grant-in-aid for scientific research from the Ministry of Education, Science, Sports and Culture, Japan (KAKENHI 13672319) awarded to K.N.

References

Egan, T.M., Haines, W.R., Voigt, M.M., 1998. A domain contributing to the ion channel of ATP-gated $P2X_2$ receptors identified by the substituted cysteine accessibility method. J. Neurosci. 18, 2350–2359.

Ennion, S., Hagan, S., Evans, R.J., 2000. The role of positively charged amino acids in ATP recognition by human $P2X_1$ receptors. J. Biol. Chem. 275, 29361–29367.

Hille, B., 1992a. Classical biophysics of the squid giant axon. Ionic Channels of Excitable Membranes, second edition. Sinauer, Sunderland, MA, pp. 23–58.

Hille, B., 1992b. Ligand-gated channels of fast chemical synapses. Ionic Channels of Excitable Membranes, second edition. Sinauer, Sunderland, MA, pp. 140–169.

Hodgkin, A.L., Huxley, A.F., 1952. The dual effect of membrane potential on sodium conductance in the giant axon of *Loligo*. J. Physiol. 116, 497–506.

Jiang, L.H., Rassendren, F., Surprenant, A., North, R.A., 2000. Identification of amino acid residues contributing to the ATP-binding site of a purinergic P2X receptor. J. Biol. Chem. 275, 34190–34196.

Katz, B., Thesleff, S., 1957. A study of the "desensitization" produced by acetylcholine at the motor end-plate. J. Physiol. 138, 63–80.

Khakh, B.S., 2001. Molecular physiology of P2X receptors and ATP signalling at synapses. Nat. Rev. 2, 165–174.

Khakh, B.S., Smith, W.B., Chiu, C.-S., Ju, D., Davidson, N., Lester, H.A., 2001. Activation-dependent changes in receptor distribution and dendritic morphology in hippocampal neurons expressing $P2X_2$-green fluorescent protein receptors. Proc. Natl. Acad. Sci. U. S. A. 98, 5288–5293.

Li, G.-H., Lee, E.M., Blair, D., Holding, C., Poronnik, P., Cook, D.I., Barden, J.A., Bennett, M.R., 2000. The distribution of P2X receptor clusters on individual neurons in sympathetic ganglia and their redistribution on agonist activation. J. Biol. Chem. 275, 29107–29112.

Nakazawa, K., Ohno, Y., 1996. Dopamine and 5-hydroxytryptamine selectively potentiate neuronal type ATP receptor channels. Eur. J. Pharmacol. 296, 119–122.

Nakazawa, K., Ohno, Y., Inoue, K., 1998. An aspartic acid residue near the second transmembrane segment of ATP receptor/channel regulates agonist sensitivity. Biochem. Biophys. Res. Commun. 244, 599–603.

Nakazawa, K., Sawa, H., Ojima, H., Ishii-Nozawa, R., Takeuchi, K., Ohno, Y., 2002. Size of side-chain at channel pore mouth affects Ca^{2+} block of $P2X_2$ receptor. Eur. J. Pharmacol. 449, 207–211.

North, R.A., 2002. Molecular physiology of P2X receptors. Physiol. Rev. 82, 1013–1067.

Ralevic, V., Burnstock, G., 1998. Receptors for purines and pyrimidines. Pharmacol. Rev. 50, 413–492.

Rassendren, F., Buell, G., Newbolt, A., North, R.A., Surprenant, A., 1997. Identification of amino acid residues contributing to the pore of a P2X receptor. EMBO J. 16, 3446–3454.

Tallarida, R.J., Jacob, L.S., 1979. Kinetics of drug–receptor interaction: interpreting dose–response data. Dose–response relation in Pharmacology. Springer, New York, NY, pp. 49–84.

Werner, P., Seward, E.P., Buell, G.N., North, R.A., 1996. Domains of P2X receptors involved in desensitization. Proc. Natl. Acad. Sci. U. S. A. 93, 15485–15490.